FISEVIER

Contents lists available at ScienceDirect

Journal of Computational Physics

www.elsevier.com/locate/jcp



A phase field model for mass transport with semi-permeable interfaces



Yuzhe Qin a,b,c, Huaxiong Huang a,e,f,*, Yi Zhu f, Chun Liu g, Shixin Xu d,**

- ^a Research Center for Mathematics, Beijing Normal University, Zhuhai 519087, China
- ^b Laboratory of Mathematics and Complex Systems (Ministry of Education), School of Mathematical Sciences, Beijing Normal University, Beijing 100875, China
- ^c School of Mathematical Sciences, Shanxi University, Taiyuan 030006, China
- ^d Zu Chongzhi Center for Mathematics and Computational Sciences (CMCS), Global Health Research Center (GHRC), Duke Kunshan University, 8 Duke Ave, Kunshan, Jiangsu, China
- ^e Beijing Normal University-Hong Kong Baptist University United International College, Zhuhai 519087, China
- f Department of Mathematics and Statistics, York University, Toronto, Ontario, Canada
- g Department of Applied Mathematics, Illinois Institute of Technology, IL 60616, USA

ARTICLE INFO

Article history: Received 28 March 2021 Received in revised form 11 May 2022 Accepted 23 May 2022 Available online 26 May 2022

Keywords: Phase field method Mass transport Restricted diffusion Sharp interface limit

ABSTRACT

In this paper, a thermaldynamical consistent model for mass transfer across permeable moving interfaces is proposed by using the energy variation method. We consider a restricted diffusion problem where the flux across the interface depends on its conductance and the difference of the concentration on each side. The diffusive interface phasefield framework used here has several advantages over the sharp interface method. First of all, explicit tracking of the interface is no longer necessary. Secondly, interfacial conditions can be incorporated with a variable diffusion coefficient. Finally, topological changes of interfaces can be handed easily. A detailed asymptotic analysis confirms the diffusive interface model converges to the existing sharp interface model as the interface thickness goes to zero. An energy stable numerical scheme is developed to solve this highly nonlinear coupled system. Numerical simulations first illustrate the consistency of theoretical results on the sharp interface limit. Then a convergence study and energy decay test are conducted to ensure the efficiency and stability of the numerical scheme. To illustrate the effectiveness of our phase-field approach, several examples are provided, including a study of a two-phase mass transfer problem where droplets with deformable interfaces are suspended in a moving fluid.

© 2022 Elsevier Inc. All rights reserved.

1. Introduction

Mass transfer through a semi-permeable or conducting interface is a common phenomenon in biology [17,12] and material science [11,18]. A representative example is that cell membranes are permeable to oxygen [33], ATP [42] and ions [22,24]. In this case, the domain consists of intracellular space denoted by Ω^+ and extracellular space denoted by Ω^- with a cell membrane Γ in between (see Fig. 1). The transport process can be described by the following diffusion equation in

E-mail addresses: hhuang@uic.edu.cn (H. Huang), shixin.xu@dukekunshan.edu.cn (S. Xu).

^{*} Corresponding author at: Duke Kunshan University, 8 Duke Ave, Kunshan, Jiangsu, China.

^{**} Corresponding author.

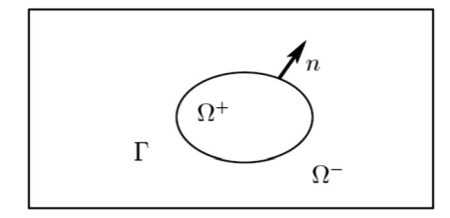


Fig. 1. Schematic of mass transport across the membrane.

the bulk [37],

$$\frac{\partial c^{\pm}}{\partial t} + \nabla \cdot (\mathbf{u}^{\pm} c^{\pm}) = \nabla \cdot (D^{\pm} \nabla c^{\pm}), \tag{1.1}$$

where c^{\pm} , \mathbf{u}^{\pm} and D^{\pm} are the concentration of the molecule, velocity of fluid and the diffusion coefficient in Ω^{\pm} , respectively. Here c^{\pm} may be discontinuous cross the boundary, like the ion concentrations in [30]. At the interface Γ , the trans-membrane flux is set to be continuous

$$-D^{+}\nabla c^{+} \cdot \mathbf{n} = -D^{-}\nabla c^{-} \cdot \mathbf{n} = K \llbracket Q(c) \rrbracket, \tag{1.2}$$

where K is the permeability, $[\![f]\!] = f^+ - f^-$ denotes the jump of concentration across the interface and n is the unit normal vector of the interface. Here Q(c) can take a variety of functional forms, such as Q(c) = c in [12] or $Q(c) = \ln c$ in [37].

For fluid-structure interaction problems, a variety of methods have been developed over the past decades. There are two most popular classes of techniques, the sharp interface methods, including the level set methods [1], immerse boundary method [23], immerse interface method [20], front tracking method [31], diffusive interface (or phase field) method [41] and boundary integral method [29]. For mass-transfer across liquid-gas interface, volume of fluid and immerse interface methods have been proposed for phase change problems [34,8], CO₂/N₂-water system [21] and water transport across a moving interface [19].

The immerse boundary method, due to its simplicity, has been applied to many fluid flow problems and has become one of the main numerical techniques for scientific computation. Gong and Huang et al. [12,33] extended the immersed boundary framework by including mass transfer in order to understand oxygen transport across permeable membranes. In order to ensure the restrict diffusion on the membrane (1.2), an additional equation is introduced to describe the temporal evolution of diffusive flux.

Unlike sharp interface methods, where the interface are handled separately by using δ function or local reconstruction, the diffusive interface method models the two phase flow and the interface in a uniform way by a label function ϕ [4,3,5]. The basic idea can be dated back to van der Waals in the late 19th century [32]. The main advantage of diffusive interface method is that it follows the energy dissipation law such that the obtained model is thermal-dynamical consistent. This makes it possible to design efficient energy stable schemes for long time simulation. However, to our best knowledge, there is not a diffusive interface model for mass transport through a semi-permeable membrane. The main challenge is how to impose the restricted diffusion near interface such that as interface thickness goes to zero, the sharp interface limit is consistent with interface condition (1.2).

In this paper, a thermal-dynamical consistent diffusive model is proposed by using energy variational method [28], which starts from two functionals for the total energy and dissipation, together with the kinematic equations based on physical laws of conservation. The key is to modify the diffusion coefficient as a function of ϕ and interface permeability K. The restricted diffusion is modelled by a changing rate of energy near the interface, following a specific dissipation rate functional. Following Xu et al. [39], a detailed asymptotic analysis confirms that the proposed diffusive interface model converges to the existing sharp interface model (1.1) and (1.2) as the interface thickness goes to zero. Based on the energy dissipation law, an efficient energy stable scheme is proposed to solve the obtained system numerically.

The structure of the paper is as follows. In section 2, a phase field model for mass transport through a semi-permable interface is proposed by using energy variational method. In section 3, the sharp interface limits of the phase field model are presented by asymptotic analysis. A decoupled, linear and unconditional energy stable numerical scheme is developed in section 4 by means of a stabilization technique and pressure correction method. In section 5, numerical experiments are carried out to validate our theoretical results and explore the effect of the membrane permeability. Finally, conclusions are drawn in section 6.

2. Phase field model for mass transfer with hydrodynamics

In this section, energy variation method is used to derive our diffusive interface model for mass transport through a semi-permeable membrane with restricted diffusion.

2.1. Model derivation

First, phase field variable ϕ is introduced to label the entire domain,

$$\phi(\mathbf{x},t) = \begin{cases} 1, & \text{in } \Omega^+, \\ -1, & \text{in } \Omega^-. \end{cases}$$
 (2.1)

The interface between the two domains is described by the zero level set $\Gamma = \{x : \phi(x, t) = 0\}$.

We start from the following kinematic assumptions on the laws of conservation: in domain $\Omega = \Omega^+ \cup \Omega^-$

$$\frac{\mathbf{D}\phi}{\mathbf{D}t} = -\nabla \cdot \mathbf{j}_{\phi},\tag{2.2a}$$

$$\frac{\mathbf{D}c}{\mathbf{p}_t} = -\nabla \cdot \mathbf{j}_c,\tag{2.2b}$$

$$\rho \frac{\mathbf{D}u}{\mathbf{p}_{t}} = \nabla \cdot \sigma_{\nu} + \nabla \cdot \sigma_{\phi}, \tag{2.2c}$$

$$\nabla \cdot \mathbf{u} = 0, \tag{2.2d}$$

where ρ is the density, c is the concentration of a substance, \boldsymbol{u} is the fluid velocity, and $\frac{\mathbf{D}f}{\mathbf{D}t} = \frac{\partial f}{\partial t} + (\boldsymbol{u} \cdot \nabla)f$ is the material derivative. Here, \boldsymbol{j}_{ϕ} and \boldsymbol{j}_{c} are two unknown mass flux of label function and concentration of the substance, respectively. σ_{ν} and σ_{ϕ} are two unknown stresses induced by the viscosity of the fluid and by two-phase flow interface, respectively. Eq. (2.2a) and Eq. (2.2b) are the conservation of mass for label function and the substance; Eq. (2.2c) is the conservation of momentum of the fluid; Eq. (2.2d) is the incompressibility of the fluid.

The boundary conditions are given as

$$\mathbf{j}_{\phi} \cdot \mathbf{n}|_{\partial\Omega} = 0, \quad \mathbf{j}_{c} \cdot \mathbf{n}|_{\partial\Omega} = 0, \quad \nabla \phi \cdot \mathbf{n}|_{\partial\Omega} = 0, \quad \mathbf{u}|_{\partial\Omega} = 0,$$
 (2.3)

where \mathbf{n} is the outward normal on the domain boundary $\partial\Omega$. Then system (2.2) conserves the local mass density, i.e. $\frac{\mathrm{d}}{\mathrm{d}t}\int_{\Omega}c\mathrm{d}\mathbf{x}=0$ and $\frac{\mathrm{d}}{\mathrm{d}t}\int_{\Omega}\phi\mathrm{d}\mathbf{x}=0$.

The total energy consists of kinetic, entropy and phase mixing energy

$$E_{total} = E_{kin} + E_{ent} + E_{mix} = \frac{1}{2} \int_{\Omega} \rho |\boldsymbol{u}|^2 d\boldsymbol{x} + \int_{\Omega} RTc(\ln\frac{c}{c_0} - 1)d\boldsymbol{x} + \int_{\Omega} \lambda (G(\phi) + \frac{\gamma^2}{2} |\nabla \phi|^2) d\boldsymbol{x}, \tag{2.4}$$

where $G(\phi) = \frac{1}{4}(1-\phi^2)^2$ is the double well potential. R is the universal gas constant, T is the thermodynamic temperature, c_0 is the reference concentration, λ is the density of phase mixing energy, γ is the thickness of the interface.

Corresponding to the total energy, we could define the chemical potentials

$$\mu_c = \frac{\delta E}{\delta c} = RT \ln \frac{c}{c_0},\tag{2.5}$$

$$\mu_{\phi} = \frac{\delta E}{\delta \phi} = -\lambda \gamma^2 \Delta \phi + \lambda G'(\phi). \tag{2.6}$$

The dissipative functional consists of fluid friction, and irreversible mixing of the substance and two phases in the bulk

$$\Delta = \int_{\Omega} 2\nu(\phi)|D_{\nu}|^{2} d\mathbf{x} + \int_{\Omega} \frac{Dc}{RT} |\nabla \mu_{c}|^{2} d\mathbf{x} + \int_{\Omega} \mathcal{M}|\nabla \mu_{\phi}|^{2} d\mathbf{x}.$$
(2.7)

where $\nu(\phi)$ is the viscosity of the fluid, $D_{\nu} = \frac{\nabla u + (\nabla u)^T}{2}$ is the strain rate, \mathcal{M} is the phenomenological mobility. In order to model restricted diffusion due to the permeability of the interface, the diffusion coefficient D is given as

$$\frac{1}{D} = \frac{(1 - \phi^2)^2}{AKq\gamma} + \frac{1 - \phi}{2D_-} + \frac{1 + \phi}{2D_+},\tag{2.8}$$

where K is the permeability for the membrane, A is a constant to be determined, $q = \frac{dQ}{dc}$ and D_+ and D_- are the diffusion coefficients in domain Ω^+ and Ω^- respectively.

Remark 2.1. First, the harmonic average form is used for the effective diffusion in Eq. (2.8) due to the continuity of the flux across the boundary. Also, in the bulk region, i.e. $\phi = \pm 1$, the effective diffusion is $D = D^{\pm}$. Near the interface, i.e. $\phi = 0$, the first term on the right is the leading term such that the membrane permeability K dominates due to small parameter γ . The unknown constant A will be shown in next Section such that the sharp interface limit of the phase field model is Eq. (1.1) with interface condition Eq. (1.2).

The energy dissipative law [9,37,28] states that without external force acting on the system, the changing rate of total energy equals the dissipation

$$\frac{\mathrm{d}}{\mathrm{d}t}E_{total} = -\Delta. \tag{2.9}$$

The definition of total energy functional (2.4) yields

$$\frac{dE_{tot}}{dt} = \frac{dE_{ent}}{dt} + \frac{dE_{kin}}{dt} + \frac{dE_{mix}}{dt}$$

$$= I_1 + I_2 + I_3.$$
(2.10)

By using the definitions of chemical potential (2.5) and conservation law (2.2b), the first term yields

$$I_{1} = \int_{\Omega} \mu_{c} \left(\frac{\partial c}{\partial t} \right) d\mathbf{x} = \int_{\Omega} \mu_{c} \left(\frac{Dc}{dt} - \mathbf{u} \cdot \nabla c \right) d\mathbf{x}$$

$$= -\int_{\Omega} \mu_{c} \nabla \cdot \mathbf{j}_{c} d\mathbf{x}$$

$$= -\int_{\partial \Omega} \mu_{c} \mathbf{j}_{c} \cdot \mathbf{n} d\mathbf{x} + \int_{\Omega} \nabla \mu_{c} \cdot \mathbf{j}_{c} d\mathbf{x}$$

$$= \int_{\Omega} \nabla \mu_{c} \cdot \mathbf{j}_{c} d\mathbf{x}, \qquad (2.11)$$

where the nonflux boundary condition for j_c and incompressibility are used here.

For the second term, by using Eqs. (2.2c) and (2.2d), we have

$$I_{2} = \frac{\mathrm{d}}{\mathrm{d}t} \left(\frac{1}{2} \int_{\Omega} \rho |\mathbf{u}|^{2} d\mathbf{x}\right)$$

$$= \frac{1}{2} \int_{\Omega} \frac{\partial \rho}{\partial t} |\mathbf{u}|^{2} d\mathbf{x} + \int_{\Omega} \rho \mathbf{u} \cdot \frac{\partial \mathbf{u}}{\partial t} d\mathbf{x}$$

$$= \frac{1}{2} \int_{\Omega} \frac{\partial \rho}{\partial t} |\mathbf{u}|^{2} d\mathbf{x} + \int_{\Omega} \rho \mathbf{u} \cdot \frac{\mathbf{D}\mathbf{u}}{\mathbf{D}t} d\mathbf{x} + \int_{\Omega} \nabla \cdot (\rho \mathbf{u}) \frac{|\mathbf{u}|^{2}}{2} d\mathbf{x}$$

$$= \int_{\Omega} \mathbf{u} \cdot (\nabla \cdot \sigma_{\eta} + \nabla \cdot \sigma_{\phi}) d\mathbf{x} - \int_{\Omega} p \nabla \cdot \mathbf{u} d\mathbf{x}$$

$$= -\int_{\Omega} \nabla \mathbf{u} : (\sigma_{\eta} + \sigma_{\phi}) d\mathbf{x} - \int_{\Omega} p \nabla \cdot \mathbf{u} d\mathbf{x}.$$
(2.12)

where pressure is induced as a Lagrange multiplier for incompressibility.

The last term is calculated with Eqs. (2.2a) and (2.6)

$$I_{3} = \frac{\mathrm{d}}{\mathrm{d}t} \int_{\Omega} (G(\phi) + \frac{\gamma^{2}}{2} |\nabla \phi|^{2}) d\mathbf{x}$$

$$= \int_{\Omega} (G'(\phi) \frac{\partial \phi}{\partial t} + \gamma^{2} \nabla \phi \cdot \nabla \frac{\partial \phi}{\partial t}) d\mathbf{x}$$

$$= \int_{\Omega} G'(\phi) \frac{\partial \phi}{\partial t} d\mathbf{x} + \int_{\partial \Omega} \gamma^{2} \frac{\partial \phi}{\partial \mathbf{n}} \frac{\partial \phi}{\partial t} d\mathbf{s} - \int_{\Omega} \nabla \cdot (\gamma^{2} \nabla \phi) \frac{\partial \phi}{\partial t} d\mathbf{x}$$

$$= \int_{\Omega} (G'(\phi) - \nabla \cdot (\gamma^{2} \nabla \phi)) \frac{\partial \phi}{\partial t} d\mathbf{x}$$

$$= \int_{\Omega} \mu_{\phi} \left(\frac{\partial \phi}{\partial t} + \mathbf{u} \cdot \nabla \phi \right) d\mathbf{x} - \int_{\Omega} \mu_{\phi} \mathbf{u} \cdot \nabla \phi d\mathbf{x}$$

$$\begin{split} &= -\int_{\Omega} \mu_{\phi} \nabla \cdot \mathbf{j}_{\phi} \mathrm{d}\mathbf{x} - \int_{\Omega} \mu_{\phi} \mathbf{u} \cdot \nabla \phi \mathrm{d}\mathbf{x} \\ &= \int_{\Omega} \nabla \mu_{\phi} \cdot \mathbf{j}_{\phi} \mathrm{d}\mathbf{x} - \int_{\partial \Omega} \mu_{\phi} \mathbf{j}_{\phi} \cdot \mathbf{n} \mathrm{d}\mathbf{s} - \int_{\Omega} (G(\phi) - \nabla \cdot (\gamma^{2} \nabla \phi)) \mathbf{u} \cdot \nabla \phi \mathrm{d}\mathbf{x} \\ &= \int_{\Omega} \nabla \mu_{\phi} \cdot \mathbf{j}_{\phi} \mathrm{d}\mathbf{x} - \int_{\Omega} \mathbf{u} \cdot \nabla G(\phi) \mathrm{d}\mathbf{x} + \int_{\Omega} \gamma^{2} \Delta \phi \nabla \phi \cdot \mathbf{u} \mathrm{d}\mathbf{x} \\ &= \int_{\Omega} \nabla \mu_{\phi} \cdot \mathbf{j}_{\phi} \mathrm{d}\mathbf{x} - \int_{\Omega} \mathbf{u} \cdot \nabla G(\phi) \mathrm{d}\mathbf{x} + \int_{\Omega} \gamma^{2} (\nabla \cdot (\nabla \phi \otimes \nabla \phi) - \frac{1}{2} \nabla |\nabla \phi|^{2}) \cdot \mathbf{u} \mathrm{d}\mathbf{x} \\ &= \int_{\Omega} \nabla \mu_{\phi} \cdot \mathbf{j}_{\phi} \mathrm{d}\mathbf{x} - \int_{\Omega} \mathbf{u} \cdot \nabla (G(\phi) + \frac{\gamma^{2}}{2} |\nabla \phi|^{2}) \mathrm{d}\mathbf{x} + \int_{\Omega} \gamma^{2} \nabla \cdot (\nabla \phi \otimes \nabla \phi) \cdot \mathbf{u} \mathrm{d}\mathbf{x} \\ &= \int_{\Omega} \nabla \mu_{\phi} \cdot \mathbf{j}_{\phi} \mathrm{d}\mathbf{x} - \int_{\Omega} \nabla \cdot (\mathbf{u} (G(\phi) + \frac{\gamma^{2}}{2} |\nabla \phi|^{2})) \mathrm{d}\mathbf{x} + \int_{\Omega} (G(\phi) + \frac{\gamma^{2}}{2} |\nabla \phi|^{2}) \nabla \cdot \mathbf{u} \mathrm{d}\mathbf{x} \\ &+ \int_{\Omega} \gamma^{2} \nabla \cdot (\nabla \phi \otimes \nabla \phi) \cdot \mathbf{u} \mathrm{d}\mathbf{x} \\ &= \int_{\Omega} \nabla \mu_{\phi} \cdot \mathbf{j}_{\phi} \mathrm{d}\mathbf{x} - \int_{\partial \Omega} (G(\phi) + \frac{\gamma^{2}}{2} |\nabla \phi|^{2})) \mathbf{u} \cdot \mathbf{n} \mathrm{d}\mathbf{s} + \int_{\Omega} \gamma^{2} \nabla \cdot (\nabla \phi \otimes \nabla \phi) \cdot \mathbf{u} \mathrm{d}\mathbf{x} \\ &= \int_{\Omega} \nabla \mu_{\phi} \cdot \mathbf{j}_{\phi} \mathrm{d}\mathbf{x} - \int_{\partial \Omega} (G(\phi) + \frac{\gamma^{2}}{2} |\nabla \phi|^{2})) \mathbf{u} \cdot \mathbf{n} \mathrm{d}\mathbf{s} + \int_{\Omega} \gamma^{2} \nabla \cdot (\nabla \phi \otimes \nabla \phi) \cdot \mathbf{u} \mathrm{d}\mathbf{x} \\ &= \int_{\Omega} \nabla \mu_{\phi} \cdot \mathbf{j}_{\phi} \mathrm{d}\mathbf{x} - \int_{\partial \Omega} \gamma^{2} (\nabla \phi \otimes \nabla \phi) : \nabla \mathbf{u} \mathrm{d}\mathbf{x}, \end{split}$$

where the nonflux boundary of ${m j}_\phi$ is used.

Substituting above three equations into Eq. (2.10) yields

$$\frac{\mathrm{d}}{\mathrm{d}t}E_{total} = \frac{\mathrm{d}}{\mathrm{d}t}E_{ent} + \frac{\mathrm{d}}{\mathrm{d}t}E_{kin} + \frac{\mathrm{d}}{\mathrm{d}t}E_{mix}$$

$$= \int_{\Omega} \nabla \mu_{c} \cdot \mathbf{j}_{c} d\mathbf{x} - \int_{\Omega} \nabla \mathbf{u} : (\sigma_{v} + \sigma_{\phi}) d\mathbf{x} - \int_{\Omega} p \nabla \cdot \mathbf{u} d\mathbf{x} + \int_{\Omega} \nabla \mu_{\phi} \cdot \mathbf{j}_{\phi} d\mathbf{x} - \int_{\Omega} \gamma^{2} (\nabla \phi \otimes \nabla \phi) : \nabla \mathbf{u} d\mathbf{x}$$

$$= -\int_{\Omega} \frac{Dc}{RT} |\nabla \mu_{c}|^{2} d\mathbf{x} - \int_{\Omega} \mathcal{M} |\nabla \mu_{\phi}|^{2} d\mathbf{x} - \int_{\Omega} 2v |D_{v}|^{2} d\mathbf{x}.$$
(2.14)

Comparing the terms in both sides of Eq. (2.14) and calculating the functional deriative, we obtain

$$\mathbf{j}_{\phi} = -\mathcal{M}\nabla\mu_{\phi},$$
 (2.15a)

$$\mathbf{j}_{c} = -\frac{Dc}{RT} \nabla \mu_{c},\tag{2.15b}$$

$$\sigma_{\nu} = 2\nu D_{\nu} - p\mathbf{I},\tag{2.15c}$$

$$\sigma_{\phi} = -\lambda \gamma^2 (\nabla \phi \otimes \nabla \phi). \tag{2.15d}$$

A diffusive interface model for mass transport through semi-permeable membrane with restricted diffusion is summarized as follows

$$\frac{\mathbf{D}\phi}{\mathbf{D}t} = \nabla \cdot (\mathcal{M}\nabla \mu_{\phi}),\tag{2.16a}$$

$$\frac{\mathbf{D}c}{\mathbf{D}t} = -\nabla \cdot \mathbf{j_c},\tag{2.16b}$$

$$\rho \frac{\mathbf{D}\boldsymbol{u}}{\mathbf{D}t} = \nabla \cdot (\nu \nabla \boldsymbol{u}) - \nabla p - \lambda \gamma^2 \nabla \cdot (\nabla \phi \otimes \nabla \phi), \tag{2.16c}$$

$$\nabla \cdot \mathbf{u} = 0, \tag{2.16d}$$

$$\mu_{\phi} = -\lambda \gamma^2 \nabla^2 \phi + \lambda G'(\phi), \tag{2.16e}$$

$$j_c = -D\nabla c,$$
 (2.16f)

$$D^{-1} = \frac{(1 - \phi^2)^2}{AKq\gamma} + \frac{1 - \phi}{2D_-} + \frac{1 + \phi}{2D_+},\tag{2.16g}$$

with boundary conditions

$$\nabla \phi \cdot \mathbf{n}|_{\partial \Omega} = 0, \quad \nabla c \cdot \mathbf{n}|_{\partial \Omega} = 0, \quad \nabla \mu \cdot \mathbf{n}|_{\partial \Omega} = 0, \quad \mathbf{u}|_{\partial \Omega} = 0. \tag{2.17}$$

2.2. Non-dimensionalization

Now we introduce the dimensionless variables

$$\tilde{\mathbf{x}} = \frac{\mathbf{x}}{L}, \quad \tilde{\mathbf{u}} = \frac{\mathbf{u}}{U}, \quad \tilde{\mathbf{t}} = \frac{t}{T}, \quad \tilde{\mathbf{c}} = \frac{c}{c_0}, \quad \tilde{K} = \frac{KL}{D_0}, \quad \tilde{D} = \frac{D}{D_0}, \quad T = \frac{L}{U}.$$
 (2.18)

Here L, T, c_0 , U D_0 are the characteristic length, time, concentration, velocity and diffusion coefficient. For convenience, the tilde symbol will be removed in the dimensionless quantities, and the dimensionless version of (2.16) is given by

$$Re\left(\frac{\partial \mathbf{u}}{\partial t} + (\mathbf{u} \cdot \nabla)\mathbf{u}\right) + \nabla p = \nabla^2 \mathbf{u} + \frac{1}{Ca}\mu\nabla\phi,\tag{2.19a}$$

$$\nabla \cdot \mathbf{u} = 0, \tag{2.19b}$$

$$\frac{\partial \phi}{\partial t} + (\mathbf{u} \cdot \nabla)\phi = \nabla \cdot (\mathcal{M}\nabla\mu),\tag{2.19c}$$

$$\mu = -\epsilon \nabla^2 \phi + \frac{1}{\epsilon} \phi(\phi^2 - 1), \tag{2.19d}$$

$$\frac{\partial c}{\partial t} + (\boldsymbol{u} \cdot \nabla)c = -\frac{1}{P_{\boldsymbol{\rho}}} \nabla \cdot \boldsymbol{j},\tag{2.19e}$$

$$\mathbf{j} = -D\nabla c,\tag{2.19f}$$

$$D^{-1} = \frac{(1 - \phi^2)^2}{AKq\epsilon} + \frac{1 - \phi}{2D^-} + \frac{1 + \phi}{2D^+},\tag{2.19g}$$

with the boundary condition

$$\mathbf{u}|_{\partial\Omega} = 0, \quad \nabla\phi \cdot \mathbf{n}|_{\partial\Omega} = 0, \quad \nabla\mu \cdot \mathbf{n}|_{\partial\Omega} = 0, \quad \nabla c \cdot \mathbf{n}|_{\partial\Omega} = 0.$$
 (2.20)

with the dimensionless parameters

$$\epsilon = \frac{\gamma}{L}, \quad Re = \frac{\rho UL}{\nu}, \quad Ca = \frac{\nu U}{\lambda \gamma}, \quad Pe = \frac{UL}{D_0}.$$
 (2.21)

Remark 2.2. In the non-dimensionalization procedure, we use the fact that

$$\begin{split} &\nabla \cdot (\nabla \phi \otimes \nabla \phi) \\ = &\nabla^2 \phi \nabla \phi + \frac{1}{2} \nabla |\nabla \phi|^2 \\ = &- \mu \nabla \phi + \frac{1}{2} \nabla \Big(|\nabla \phi|^2 + \frac{1}{\epsilon} G(\phi) \Big), \end{split}$$

and redefine pressure function

$$p = p + \frac{\epsilon}{2Ca} |\nabla \phi|^2 + \frac{1}{2Ca} G(\phi).$$

Theorem 2.1. If ϕ , c, u and p are smooth solutions of the system (2.19) with boundary condition (2.20), then the following energy law is satisfied:

$$\frac{\mathrm{d}}{\mathrm{d}t}\mathcal{E}_{total} = -\int_{\Omega} \left(|\nabla \boldsymbol{u}|^2 + \frac{\mathcal{M}}{Ca} |\nabla \mu|^2 + Dc |\nabla \mu_c|^2 \right) \mathrm{d}\boldsymbol{x},\tag{2.22}$$

where

$$\mathcal{E}_{total} = \int_{\Omega} \left(\frac{Re}{2} |\boldsymbol{u}|^2 + \frac{1}{Ca} \left(\frac{\epsilon}{2} |\nabla \phi|^2 + \frac{1}{4\epsilon} (1 - \phi^2)^2 \right) + c \ln c \right) d\boldsymbol{x}. \tag{2.23}$$

Proof. By taking the L^2 inner product of (2.19a), (2.19c), (2.19d), (2.19e) and (2.19f) with \boldsymbol{u} , μ , $\frac{\partial \phi}{\partial t}$, μ_c and $\frac{\partial c}{\partial t}$ respectively, one obtains immediately (2.22).

3. Sharp interface limit

In this section, a detailed asymptotic analysis is presented by using the results in [39] to show that the sharp interface limits of the obtained system (2.19). Here we assume viscosity is a constant and $\mathcal{M}=\alpha\epsilon^2$, where α is a constant independent of ϵ .

3.1. Outer expansions

Far from the two-phase interface Γ , we use the following ansatz:

$$\mathbf{u}_{\epsilon}^{\pm} = \mathbf{u}_{0}^{\pm} + \epsilon \mathbf{u}_{1}^{\pm} + \epsilon^{2} \mathbf{u}_{2}^{\pm} + o(\epsilon^{2}), \tag{3.1a}$$

$$p_{\epsilon}^{\pm} = p_0^{\pm} + \epsilon p_1^{\pm} + \epsilon^2 p_2^{\pm} + o(\epsilon^2),$$
 (3.1b)

$$\phi_{\epsilon}^{\pm} = \phi_0^{\pm} + \epsilon \phi_1^{\pm} + \epsilon^2 \phi_2^{\pm} + o(\epsilon^2), \tag{3.1c}$$

$$\mu_{\epsilon}^{\pm} = \epsilon^{-1} \mu_{0}^{\pm} + \mu_{1}^{\pm} + \epsilon \mu_{2}^{\pm} + o(\epsilon), \tag{3.1d}$$

$$c_{\epsilon}^{\pm} = c_0^{\pm} + \epsilon c_1^{\pm} + \epsilon^2 c_2^{\pm} + o(\epsilon^2), \tag{3.1e}$$

$$\mathbf{j}_{\epsilon}^{\pm} = \mathbf{j}_{0}^{\pm} + \epsilon \, \mathbf{j}_{1}^{\pm} + \epsilon^{2} \, \mathbf{j}_{2}^{\pm} + o(\epsilon^{2}). \tag{3.1f}$$

The leading order of Navier-Stokes-Cahn-Hilliard system is

$$\frac{\partial \phi_0^{\pm}}{\partial t} + \nabla \cdot (\mathbf{u}_0^{\pm} \phi_0^{\pm}) = 0, \tag{3.2a}$$

$$\mu_0^{\pm} \nabla \phi_0^{\pm} = 0,$$
 (3.2b)

$$\nabla \cdot \boldsymbol{u}_0^{\pm} = 0, \tag{3.2c}$$

$$\frac{\partial \phi_0^{\pm}}{\partial t} + \nabla \cdot (\mathbf{u}^{\pm} \phi_0^{\pm}) = \alpha \triangle \mu_0^{\pm} \tag{3.2d}$$

$$\mu_0^{\pm} = (\phi_0^{\pm})^3 - \phi_0^{\pm}.$$
 (3.2e)

Combining Eqs. (3.2b) and (3.2e) yields [39]

$$\phi_0^{\pm} = C_0^{\pm},\tag{3.3a}$$

$$\mu_0^{\pm} = (C_0^{\pm})^3 - C_0^{\pm}. \tag{3.3b}$$

The ϵ^0 order of Navier-Stokes equation is

$$Re\left(\frac{\partial \boldsymbol{u}_{0}^{\pm}}{\partial t} + (\boldsymbol{u}_{0}^{\pm} \cdot \nabla)\boldsymbol{u}_{0}^{\pm}\right) + \nabla p_{0}^{\pm} = \nabla^{2}\boldsymbol{u}_{0}^{\pm} + \frac{1}{Ca}\mu_{0}^{\pm}\nabla\phi_{1}^{\pm}.$$
(3.4)

Substituting (3.1e),(3.1f) into Eq. (2.19f) yields

$$\begin{split} &[2D^{+}D^{-}(1-(\phi_{0}^{\pm}+\epsilon\phi_{1}^{\pm}+\epsilon^{2}\phi_{2}^{\pm}+o(\epsilon^{2}))^{2})^{2}+AKq\epsilon(D^{+}+D^{-})\\ &+AKq\epsilon(D^{-}-D^{+})(\phi_{0}^{\pm}+\epsilon\phi_{1}^{\pm}+\epsilon^{2}\phi_{2}^{\pm}+o(\epsilon^{2}))](\boldsymbol{j}_{0}^{\pm}+\epsilon\boldsymbol{j}_{1}^{\pm}+\epsilon^{2}\boldsymbol{j}_{2}^{\pm}+o(\epsilon^{2}))\\ &=-2AK\epsilon D^{+}D^{-}[q(c_{0}^{\pm})+\epsilon q'(c_{0}^{\pm})c_{1}^{\pm}+\epsilon^{2}(\frac{1}{2}q''(c_{0}^{\pm})(c_{1}^{\pm})^{2}+q'(c_{0}^{\pm})c_{2}^{\pm})+o(\epsilon^{2})]\nabla(c_{0}^{\pm}+\epsilon c_{1}^{\pm}+\epsilon^{2}c_{2}^{\pm}+o(\epsilon^{2})), \end{split}$$

The leading order term of the above equation is

$$(1 - (\phi_0^{\pm})^2)^2 \mathbf{j}_0^{\pm} = 0, \tag{3.6}$$

and the next order term is

$$AKq(c_0^{\pm})[(D^+ + D^-) + (D^- - D^+)\phi_0^{\pm}]\boldsymbol{j}_0^{\pm} + 2D^+D^-(1 - (\phi_0^{\pm})^2)^2\boldsymbol{j}_1^{\pm} = -2AKD^+D^-q(c_0^{\pm})\nabla c_0^{\pm}. \tag{3.7}$$

The leading order of (2.19e) gives

$$\frac{\partial c_0^{\pm}}{\partial t} + \boldsymbol{u}_0^{\pm} \cdot \nabla c_0^{\pm} = -\frac{1}{P_{\boldsymbol{\theta}}} \nabla \cdot \boldsymbol{j}_0^{\pm}. \tag{3.8}$$

In summary, for the outer region, $(c_0^\pm,~\phi_0^\pm~, \pmb{u}_0^\pm, p_0^\pm)$ satisfy the following system

$$\frac{\partial c_0^{\pm}}{\partial t} + \boldsymbol{u}_0^{\pm} \cdot \nabla c_0^{\pm} = -\frac{1}{P_{\boldsymbol{\rho}}} \nabla \cdot \boldsymbol{j}_0^{\pm}, \tag{3.9a}$$

$$Re\left(\frac{\partial \boldsymbol{u}_{0}^{\pm}}{\partial t} + (\boldsymbol{u}_{0}^{\pm} \cdot \nabla)\boldsymbol{u}_{0}^{\pm}\right) + \nabla p_{0}^{\pm} = \nabla^{2}\boldsymbol{u}_{0}^{\pm} + \frac{1}{Ca}\mu_{0}^{\pm}\nabla\phi_{1}^{\pm},\tag{3.9b}$$

$$\nabla \cdot \boldsymbol{u}_0^{\pm} = 0 \quad \text{in } \Omega^{\pm}, \tag{3.9c}$$

$$\frac{\partial \phi_0^{\pm}}{\partial t} + \nabla \cdot (\mathbf{u}_0^{\pm} \phi_0^{\pm}) = 0, \tag{3.9d}$$

$$\phi_0^{\pm} = C_0^{\pm}, \ \mu_0^{\pm} = (C_0^{\pm})^3 - C_0^{\pm}.$$
 (3.9e)

3.2. Inner expansions

We first introduce the signed distance function $d(\mathbf{x})$ to the interface Γ . Immediately, we have $\nabla d = \mathbf{n}$. After defining a new rescaled variable

$$\xi = \frac{d(\mathbf{x})}{\epsilon},\tag{3.10}$$

for any scalar function f(x), we can rewrite it as

$$f(\mathbf{x}) = \tilde{f}(\mathbf{x}, \xi), \tag{3.11}$$

and the relevant operators are

$$\nabla f(\mathbf{x}) = \nabla_{\mathbf{x}} \tilde{f} + \epsilon^{-1} \partial_{\varepsilon} \tilde{f} \mathbf{n}, \tag{3.12a}$$

$$\nabla^{2} f(\mathbf{x}) = \nabla_{\mathbf{x}}^{2} \tilde{f} + \epsilon^{-1} \partial_{\xi} \tilde{f} K + 2\epsilon^{-1} (\mathbf{n} \cdot \nabla_{\mathbf{x}}) \partial_{\xi} \tilde{f} + \epsilon^{-2} \partial_{\xi\xi} \tilde{f}, \tag{3.12b}$$

$$\partial_t f = \partial_t \tilde{f} + \epsilon^{-1} \partial_{\varepsilon} \tilde{f} \partial_t d, \tag{3.12c}$$

and for a vector function $\tilde{\boldsymbol{g}}(\boldsymbol{x})$, we have

$$\nabla \cdot \tilde{\mathbf{g}}(\mathbf{x}) = \nabla_{\mathbf{x}} \cdot \tilde{\mathbf{g}} + \epsilon^{-1} \partial_{\varepsilon} \tilde{\mathbf{g}} \cdot \mathbf{n}, \tag{3.13}$$

Here $\nabla_{\mathbf{x}}$ and $\nabla_{\mathbf{x}}^2$ are the gradient and Laplace operators with respect to \mathbf{x} , respectively. We use the fact that $\nabla_{\mathbf{x}} \cdot \mathbf{n} = \kappa$ for $\mathbf{x} \in \Gamma(t)$, the mean curvature of the interface. In the inner region, we assume that

$$\tilde{\mathbf{u}}_{\epsilon} = \tilde{\mathbf{u}}_0 + \epsilon \tilde{\mathbf{u}}_1 + \epsilon^2 \tilde{\mathbf{u}}_2 + o\left(\epsilon^2\right),\tag{3.14a}$$

$$\tilde{\phi}_{\epsilon} = \tilde{\phi}_0 + \epsilon \tilde{\phi}_1 + \epsilon^2 \tilde{\phi}_2 + o\left(\epsilon^2\right),\tag{3.14b}$$

$$\tilde{p}_{\epsilon} = \tilde{p}_0 + \epsilon \tilde{p}_1 + \epsilon^2 \tilde{p}_2 + o\left(\epsilon^2\right),\tag{3.14c}$$

$$\tilde{c}_{\epsilon} = \tilde{c}_0 + \epsilon \tilde{c}_1 + \epsilon^2 \tilde{c}_2 + o\left(\epsilon^2\right),\tag{3.14d}$$

$$\tilde{\boldsymbol{j}}_{\epsilon} = \tilde{\boldsymbol{j}}_{0} + \epsilon \tilde{\boldsymbol{j}}_{1} + \epsilon^{2} \tilde{\boldsymbol{j}}_{2} + o\left(\epsilon^{2}\right), \tag{3.14e}$$

$$\tilde{\mu}_{\epsilon} = \epsilon^{-1} \tilde{\mu}_0 + \tilde{\mu}_1 + \epsilon \tilde{\mu}_2 + o(\epsilon), \tag{3.14f}$$

where

$$\tilde{\mu}_0 = -\partial_{\xi\xi}\tilde{\phi}_0 - \tilde{\phi}_0 + \tilde{\phi}_0^3,\tag{3.15a}$$

$$\tilde{\mu}_1 = -\partial_{\xi\xi}\tilde{\phi}_1 - \partial_{\xi}\tilde{\phi}_0\kappa + 2\left(\mathbf{n}\cdot\nabla_{\mathbf{x}}\right)\partial_{\xi}\tilde{\phi}_0 - \tilde{\phi}_1 + 3\tilde{\phi}_0^2\tilde{\phi}_1. \tag{3.15b}$$

It can be shown that

$$q(\tilde{c}_{\epsilon}^{\pm}) = q(\tilde{c}_{0}^{\pm}) + \epsilon q'(\tilde{c}_{0}^{\pm})\tilde{c}_{1}^{\pm} + \epsilon^{2}(\frac{1}{2}q''(\tilde{c}_{0}^{\pm})(\tilde{c}_{1}^{\pm})^{2} + q'(\tilde{c}_{0}^{\pm})\tilde{c}_{2}^{\pm}) + o(\epsilon^{2}).$$
(3.16)

Using the results in [39], the phase field equations and Navier-Stokes equations can be transformed into the following forms:

$$\partial_{t}\tilde{\phi}_{\epsilon} + \epsilon^{-1}\partial_{\xi}\tilde{\phi}_{\epsilon}\partial_{t}d + \tilde{\mathbf{u}} \cdot (\nabla_{\mathbf{x}}\tilde{\phi}_{\epsilon} + \epsilon^{-1}\mathbf{n}\partial_{\xi}\tilde{\phi}_{\epsilon}) \\
= \mathcal{M}(\nabla_{\mathbf{x}}^{2}\tilde{\mu}_{\epsilon} + \epsilon^{-1}\partial_{\xi}\tilde{\mu}_{\epsilon}\kappa + 2\epsilon^{-1}(\mathbf{n} \cdot \nabla_{\mathbf{x}})\partial_{\xi}\tilde{\mu}_{\epsilon} + \epsilon^{-2}\partial_{\xi\xi}\tilde{\mu}_{\epsilon}), \\
\operatorname{Re}\left(\partial_{t}\tilde{\mathbf{u}}_{\epsilon} + \epsilon^{-1}\partial_{\varepsilon}\tilde{\mathbf{u}}_{\epsilon}\partial_{t}d + \tilde{\mathbf{u}} \cdot (\nabla_{\mathbf{x}}\tilde{\mathbf{u}}_{\epsilon} + \epsilon^{-1}\mathbf{n}\partial_{\varepsilon}\tilde{\mathbf{u}}_{\epsilon})\right) + \nabla_{\mathbf{x}}\tilde{\mathbf{p}}_{\epsilon} + \epsilon^{-1}\partial_{\varepsilon}\tilde{\mathbf{p}}_{\epsilon}\mathbf{n}$$
(3.17a)

$$= \nabla_{\mathbf{x}}^{2} \tilde{\mathbf{u}}_{\epsilon} + \epsilon^{-1} \partial_{\xi} \tilde{\mathbf{u}}_{\epsilon} \kappa + 2\epsilon^{-1} (\mathbf{n} \cdot \nabla_{\mathbf{x}}) \partial_{\xi} \tilde{\mathbf{u}}_{\epsilon} + \epsilon^{-2} \partial_{\xi\xi} \tilde{\mathbf{u}}_{\epsilon} + \frac{1}{Ca} \tilde{\mu}_{\epsilon} \left(\nabla_{\mathbf{x}} \tilde{\phi}_{\epsilon} + \epsilon^{-1} \partial_{\xi} \tilde{\phi}_{\epsilon} \mathbf{n} \right), \tag{3.17b}$$

The leading order terms of Eq. (3.17) are

$$(\partial_t d + \tilde{\boldsymbol{u}}_0 \cdot \boldsymbol{n}) \partial_{\xi} \tilde{\phi}_0 = \alpha \partial_{\xi\xi} \tilde{\mu}_0, \tag{3.18a}$$

$$\partial_{\xi\xi}\tilde{\mathbf{u}}_0 + \frac{1}{Ca}\tilde{\mu}_0\partial_{\xi}\tilde{\phi}_0\mathbf{n} = 0. \tag{3.18b}$$

Intergrating the first equation and using the matching condition of $\tilde{\phi}_0$, $\partial_{\xi}\tilde{\mu}_0$ yields [39]

$$\partial_t d + \tilde{\boldsymbol{u}}_0 \cdot \boldsymbol{n} = 0, \tag{3.19}$$

which means on the interface Γ

$$V_n = \mathbf{u}_0 \cdot \mathbf{n} \tag{3.20}$$

Combining Eqs. (3.18a) and (3.19) yields

$$\partial_{\xi\xi}\tilde{\mu}_0 = 0. \tag{3.21a}$$

Then combining above equations and the matching conditions yield [39]

$$\tilde{\mu}_0 = 0 \tag{3.22}$$

By the equation (3.15a), we have

$$-\partial_{\xi\xi}\tilde{\phi}_0 - \tilde{\phi}_0 + \tilde{\phi}_0^3 = 0. \tag{3.23}$$

The solvability condition for this equation leads to [39]

$$\lim_{\varepsilon \to +\infty} \tilde{\phi}_0 = \pm 1,\tag{3.24}$$

and the solution of (3.23) is

$$\tilde{\phi}_0 = \tanh \frac{\xi}{\sqrt{2}}.\tag{3.25}$$

It means

$$\phi(\mathbf{x},t) = \tanh \frac{d(\mathbf{x},t)}{\sqrt{2}\epsilon}.$$
(3.26)

This is the profile of the $\tilde{\phi}_0$ in the diffuse-interface layer. The matching condition $\lim_{\epsilon \to +\infty} \tilde{\phi}_0 = \phi_0^\pm$ gives

$$\phi_0^{\pm} = \pm 1. \tag{3.27}$$

Therefore, Eq. (3.9b) is reduced to

$$Re\left(\frac{\partial \boldsymbol{u}_0^{\pm}}{\partial t} + (\boldsymbol{u}_0^{\pm} \cdot \nabla)\boldsymbol{u}_0^{\pm}\right) + \nabla p_0^{\pm} = \nabla^2 \boldsymbol{u}_0^{\pm}. \tag{3.28}$$

Thanks to Eq. (3.27), Eq. (3.7) yields

$$\mathbf{j}_0^{\pm} = -D^{\pm} \nabla c_0^{\pm}. \tag{3.29}$$

Combining Eq. (3.22) and Eq. (3.18b) yields

$$\partial_{\varepsilon k} \tilde{\mathbf{u}}_0 = 0, \tag{3.30}$$

which means $\|\mathbf{u}_0\| = 0$ on the interface by the matching condition.

The first order of Eq. (3.17b) could be rewritten as follows

$$-\partial_{\xi}\tilde{p}_{0}\mathbf{n} + \partial_{\xi\xi}\tilde{\mathbf{u}}_{1} + \frac{1}{Ca}\tilde{\mu}_{1}\partial_{\xi}\tilde{\phi}_{0}\mathbf{n} = 0, \tag{3.31}$$

which leads to the jump condition

$$\llbracket -p_0 \mathbf{n} + (\mathbf{n} \cdot \nabla) \mathbf{u}_0 \rrbracket = \frac{1}{Ca} \sigma \kappa \mathbf{n}, \tag{3.32}$$

with the surface tension $\sigma=\int_{-\infty}^{\infty}(\partial_{\xi}\tilde{\phi}_{0})^{2}\mathrm{d}\xi=\frac{2\sqrt{2}}{3}.$ The concentration equation can be transformed into the following form

$$\partial_{t}\tilde{c}_{\epsilon} + \epsilon^{-1}\partial_{\xi}\tilde{c}_{\epsilon}\partial_{t}d + \tilde{\boldsymbol{u}}_{\epsilon} \cdot (\nabla_{\boldsymbol{x}}\tilde{c}_{\epsilon} + \epsilon^{-1}\boldsymbol{n}\partial_{\xi}\tilde{c}_{\epsilon}) = -\frac{1}{P_{P}}(\nabla_{\boldsymbol{x}}\cdot\tilde{\boldsymbol{j}}_{\epsilon} + \epsilon^{-1}\partial_{\xi}\tilde{\boldsymbol{j}}_{\epsilon}\cdot\boldsymbol{n}), \tag{3.33a}$$

$$\tilde{\boldsymbol{j}}_{\epsilon} = -\frac{2AK\epsilon D^{+}D^{-}q(\tilde{c}_{\epsilon})}{2D^{+}D^{-}(1-\tilde{\phi}_{\epsilon}^{2})^{2} + AKq\epsilon(D^{+}+D^{-}) + AKq\epsilon(D^{-}-D^{+})\tilde{\phi}_{\epsilon}}(\nabla_{\boldsymbol{x}}\tilde{c}_{\epsilon} + \epsilon^{-1}\partial_{\xi}\tilde{c}_{\epsilon}\boldsymbol{n}), \tag{3.33b}$$

The leading order term of equation (3.33a) is

$$\partial_{\xi}\tilde{c}_{0}\partial_{t}d + \tilde{\mathbf{u}}_{0} \cdot \mathbf{n}\partial_{\xi}\tilde{c}_{0} = -\frac{1}{P_{P}}\partial_{\xi}\tilde{\mathbf{j}}_{0} \cdot \mathbf{n}. \tag{3.34}$$

Using Eq. (3.19), we have

$$-\partial_{\varepsilon}\tilde{\mathbf{j}}_{0}\cdot\mathbf{n}=0\tag{3.35}$$

which means $\tilde{\boldsymbol{j}}_0 \cdot \boldsymbol{n} = \text{const.}$

Integrating the equation (3.35) in $(-\infty, \infty)$, we obtain

$$[\![\boldsymbol{j}_0 \cdot \boldsymbol{n}]\!] = -\int\limits_{-\infty}^{\infty} \partial_{\xi} \tilde{\boldsymbol{j}}_0 d\xi \cdot \boldsymbol{n} = 0.$$
(3.36)

Therefore the flux of concentration is continuous across the interface.

Eq. (3.33b) could be written as follows

$$(2D^{+}D^{-}(1-\tilde{\phi}_{\epsilon}^{2})^{2}+AKq\epsilon(D^{+}+D^{-})+AKq\epsilon(D^{-}-D^{+})\tilde{\phi}_{\epsilon})\tilde{\mathbf{j}}_{\epsilon}=-2D^{+}D^{-}AK\epsilon q(\tilde{c}_{\epsilon})(\nabla_{\mathbf{x}}\tilde{c}_{\epsilon}+\epsilon^{-1}\partial_{\epsilon}\tilde{c}_{\epsilon}\mathbf{n}).$$

and the leading order term gives us that

$$(1 - \tilde{\phi}_0^2)^2 \tilde{\mathbf{j}}_0 \cdot \mathbf{n} = -AKq(\tilde{c}_0)\partial_{\varepsilon}\tilde{c}_0. \tag{3.37}$$

Integrating this equation in $(-\infty, \infty)$ we have

$$AK \llbracket Q(c_0) \rrbracket = AK \int_{-\infty}^{+\infty} q(\tilde{c}_0) \partial_{\xi} \tilde{c}_0 d\xi$$

$$= \int_{-\infty}^{+\infty} (1 - \tilde{\phi}_0^2)^2 \tilde{\mathbf{j}}_0 \cdot \mathbf{n} d\xi$$

$$= \mathbf{j}_0 \cdot \mathbf{n} \int_{-\infty}^{+\infty} (1 - \tanh^2 \frac{\xi}{\sqrt{2}})^2 d\xi.$$
(3.38)

By setting

$$A = \int_{-\infty}^{+\infty} (1 - \tanh^2 \frac{\xi}{\sqrt{2}})^2 d\xi = \frac{4\sqrt{2}}{3} = 2\sigma.$$
 (3.39)

we obtain

$$\mathbf{j}_0 \cdot \mathbf{n} = K[[0, (c_0)]]. \tag{3.40}$$

Combining the above results, we obtain the following at the leading order

$$Re\left(\frac{\partial \boldsymbol{u}_{0}^{\pm}}{\partial t} + (\boldsymbol{u}_{0}^{\pm} \cdot \nabla)\boldsymbol{u}_{0}^{\pm}\right) + \nabla p_{0}^{\pm} = \nabla^{2}\boldsymbol{u}_{0}^{\pm}, \quad \text{in } \Omega_{\pm},$$
(3.41a)

$$\nabla \cdot \boldsymbol{u}_0^{\pm} = 0, \quad \text{in } \Omega_{\pm}, \tag{3.41b}$$

$$\frac{\partial c_0^{\pm}}{\partial t} + (\boldsymbol{u}_0^{\pm} \cdot \nabla)c_0^{\pm} = \frac{1}{P_{\boldsymbol{\theta}}} \nabla \cdot (D^{\pm} \nabla c^{\pm}), \quad \text{in } \Omega_{\pm}, \tag{3.41c}$$

$$\llbracket \boldsymbol{u}_0 \rrbracket = 0, \quad \text{on } \Gamma, \tag{3.41d}$$

$$-D^{+}\nabla c_{0}^{+} \cdot \mathbf{n} = -D^{-}\nabla c_{0}^{-} \cdot \mathbf{n} = K[[Q(c_{0})]], \quad \text{on } \Gamma,$$

$$(3.41e)$$

$$[-p_0 \mathbf{n} + (\mathbf{n} \cdot \nabla) \mathbf{u}_0] = \frac{1}{Ca} \sigma \kappa \mathbf{n}, \quad \text{on } \Gamma,$$
(3.41f)

$$V_n = \mathbf{u}_0 \cdot \mathbf{n}, \quad \text{on } \Gamma.$$
 (3.41g)

This illustrates that our diffusive interface model converges to the sharp interface model for mass transport with restricted diffusion condition (2.15b).

4. Numerical method

Equations in (2.19) form a coupled nonlinear system. In this section, we propose an unconditionally energy stable numerical scheme for our proposed mathematical model based on the stabilization method [36,26,43,27,25].

In order to assure volume conservation, we need to rearrange some terms in system (2.19) by taking into account the following relations

$$\begin{cases} \mu \nabla \phi = \nabla(\phi \mu) - \phi \nabla \mu, \\ \mathbf{u} \cdot \nabla \phi = \nabla \cdot (\phi \mathbf{u}). \end{cases}$$
(4.1)

We introduce a new pressure as

$$\tilde{p} = p - \frac{1}{Ca}\phi\mu. \tag{4.2}$$

To simplify notations, we will use p instead of \tilde{p} in the rest of the paper.

Before the semi-discrete numerical scheme, we assume that the double-well function $G(\phi)$ satisfies the following condition: there exists a constant L such that

$$\max_{|\phi| \in \mathbb{R}} |G''(\phi)| \le L. \tag{4.3}$$

It has been a common practice to consider the Cahn-Hilliard equation with a truncated double-well potential by quadratic growth at infinities (see [10,26]), so that the maximum norm of the solution for the Cahn-Hilliard equation is bounded which is proved in [2]. It is then obvious that there exists a constant L such that (4.3) is satisfied with the truncated double-well function $G(\phi)$.

Given initial conditions ϕ^0 , μ^0 , \boldsymbol{u}^0 , p^0 and c^0 , we compute $(\phi^{n+1}, \mu^{n+1}, \tilde{\boldsymbol{u}}^{n+1}, \boldsymbol{u}^{n+1}, p^{n+1}, c^{n+1})$ for $n \ge 0$ by three steps. **Step 1.** We solve for the phase field variable ϕ^{n+1} by the following scheme with the help of stabilization method and Navier-Stokes equation by pressure correction method [6.13]:

$$Re\left(\frac{\tilde{\boldsymbol{u}}^{n+1} - \boldsymbol{u}^n}{\delta t} + (\boldsymbol{u}^n \cdot \nabla)\tilde{\boldsymbol{u}}^{n+1}\right) + \nabla p^n = \Delta \tilde{\boldsymbol{u}}^{n+1} - \frac{1}{Ca}\phi^n \nabla \mu^{n+1}, \tag{4.4a}$$

$$\frac{\phi^{n+1} - \phi^n}{\delta t} + \nabla \cdot (\tilde{\boldsymbol{u}}^{n+1} \phi^n) = \nabla \cdot (\mathcal{M} \nabla \mu^{n+1}), \tag{4.4b}$$

$$\mu^{n+1} = -\epsilon \Delta \phi^{n+1} + \frac{s}{\epsilon} (\phi^{n+1} - \phi^n) + \frac{1}{\epsilon} G'(\phi^n), \tag{4.4c}$$

with the boundary condition

$$\nabla \phi^{n+1} \cdot \boldsymbol{n}|_{\partial \Omega} = 0, \quad \nabla \mu^{n+1} \cdot \boldsymbol{n}|_{\partial \Omega} = 0, \quad \tilde{\boldsymbol{u}}^{n+1}|_{\partial \Omega} = 0. \tag{4.5}$$

Step 2. We apply projection to ensure incompressiblity

$$Re\frac{\boldsymbol{u}^{n+1} - \tilde{\boldsymbol{u}}^{n+1}}{\delta t} + \nabla(p^{n+1} - p^n) = 0, \tag{4.6a}$$

$$\nabla \cdot \boldsymbol{u}^{n+1} = 0, \tag{4.6b}$$

with boundary condition

$$\mathbf{u}^{n+1}|_{\partial\Omega} = 0. \tag{4.7}$$

Step 3. We update c^{n+1} by a fully implicit Euler scheme:

$$\frac{c^{n+1} - c^n}{\delta t} + (\boldsymbol{u}^{n+1} \cdot \nabla)c^{n+1} = -\nabla \cdot \boldsymbol{j}^{n+1},\tag{4.8a}$$

$$\mathbf{j}^{n+1} = -D^{n+1}c^{n+1}\nabla\mu_c^{n+1},\tag{4.8b}$$

$$\mu_c^{n+1} = \ln c^{n+1},$$
 (4.8c)

$$\frac{1}{D^{n+1}} = \frac{(1 - (\phi^{n+1})^2)^2}{AKq(c^n)\epsilon} + \frac{1 - \phi^{n+1}}{2D^-} + \frac{1 + \phi^{n+1}}{2D^+},\tag{4.8d}$$

with boundary conditions

$$\nabla c^{n+1} \cdot \mathbf{n}|_{\partial\Omega} = 0, \quad \nabla \mu_c^{n+1} \cdot \mathbf{n}|_{\partial\Omega} = 0. \tag{4.9}$$

Theorem 4.1. If assumption (4.3) holds and let $s \ge L/2$, then system (4.4) – (4.9) is uniquely solvable, unconditionally stable and obey the following discrete energy law:

$$\frac{Re}{2}(\|\boldsymbol{u}^{n+1}\|^{2} - \|\boldsymbol{u}^{n}\|^{2}) + \frac{\delta t^{2}}{2Re}(\|\nabla p^{n+1}\|^{2} - \|\nabla p^{n}\|^{2})
+ \frac{1}{Ca}(\frac{\epsilon}{2}(\|\nabla \phi^{n+1}\|^{2} - \|\nabla \phi^{n}\|^{2}) + \frac{1}{\epsilon}(G(\phi^{n+1}) - G(\phi^{n}), 1))
+ (c^{n+1}\ln c^{n+1} - c^{n}\ln c^{n}, 1)
\leq -\delta t \|\nabla \tilde{\boldsymbol{u}}^{n+1}\|^{2} - \delta t \frac{\mathcal{M}}{Ca} \|\nabla \mu^{n+1}\|^{2} - \delta t \int_{\Omega} D^{n+1}c^{n+1}|\nabla \mu_{c}^{n+1}|^{2} d\boldsymbol{x}, \tag{4.10}$$

where $\|\cdot\|$ denotes the discrete L^2 norm in domain Ω .

Proof. Taking the inner product of equation (4.4a) with $2\delta t \tilde{\boldsymbol{u}}^{n+1}$, we have

$$Re(\|\tilde{\boldsymbol{u}}^{n+1}\|^2 - \|\boldsymbol{u}^n\|^2 + \|\tilde{\boldsymbol{u}}^{n+1} - \boldsymbol{u}^n\|^2) + \frac{2\delta t}{Ca}(\phi^n \nabla \mu^{n+1}, \tilde{\boldsymbol{u}}^{n+1}) + 2\delta t(\nabla p^n, \tilde{\boldsymbol{u}}^{n+1}) + 2\delta t\|\nabla \tilde{\boldsymbol{u}}^{n+1}\|^2 = 0. \tag{4.11}$$

We rewrite projection step (4.6a) as

$$\frac{Re}{st}\boldsymbol{u}^{n+1} + \nabla p^{n+1} = \frac{Re}{st}\tilde{\boldsymbol{u}}^{n+1} + \nabla p^{n}. \tag{4.12}$$

By squaring both sides of the above equality, we obtain

$$\frac{Re^2}{\delta t^2} \|\mathbf{u}^{n+1}\|^2 + \|\nabla p^{n+1}\|^2 = \frac{Re^2}{\delta t^2} \|\tilde{\mathbf{u}}^{n+1}\|^2 + \|\nabla p^n\|^2 + \frac{2Re}{\delta t} (\tilde{\mathbf{u}}^{n+1}, \nabla p^n), \tag{4.13}$$

namely, by multiplying $\delta t^2/Re$ for the above equation, we have

$$Re\|\mathbf{u}^{n+1}\|^2 + \frac{\delta t^2}{Re}\|\nabla p^{n+1}\|^2 = Re\|\tilde{\mathbf{u}}^{n+1}\|^2 + \frac{\delta t^2}{Re}\|\nabla p^n\|^2 + 2\delta t(\tilde{\mathbf{u}}^{n+1}, \nabla p^n). \tag{4.14}$$

By combining (4.11) and (4.14), we obtain

$$Re(\|\boldsymbol{u}^{n+1}\|^2 - \|\boldsymbol{u}^n\|^2 + \|\tilde{\boldsymbol{u}}^{n+1} - \boldsymbol{u}^n\|^2) + \frac{\delta t^2}{Re} \|\nabla p^{n+1}\|^2 - \frac{\delta t^2}{Re} \|\nabla p^n\|^2$$
(4.15)

$$+2\delta t \|\nabla \tilde{\boldsymbol{u}}^{n+1}\|^2 + \frac{2\delta t}{Ca} (\phi^n \nabla \mu^{n+1}, \tilde{\boldsymbol{u}}^{n+1}) = 0.$$
(4.16)

It now remains to deal with the last term in the above. Taking the inner product of the first equation of (4.4b) with $2\delta t \mu^{n+1}$, we get

$$2(\phi^{n+1} - \phi^n, \mu^{n+1}) - 2\delta t(\tilde{\boldsymbol{u}}^{n+1}, \mu^{n+1} \nabla \phi^n) + 2\delta t \mathcal{M} \|\nabla \mu^{n+1}\|^2 = 0.$$

$$(4.17)$$

Taking the inner product of (4.4c) with $-2(\phi^{n+1} - \phi^n)$, we obtain

Y. Qin, H. Huang, Y. Zhu et al.

$$-2(\mu^{n+1}, \phi^{n+1} - \phi^n) + \epsilon (\|\nabla \phi^{n+1}\|^2 - \|\nabla \phi^n\|^2 + \|\nabla \phi^{n+1} - \nabla \phi^n\|^2)$$

$$+ \frac{2s}{\epsilon} \|\phi^{n+1} - \phi^n\|^2 + \frac{2}{\epsilon} (G'(\phi^n), \phi^{n+1} - \phi^n) = 0.$$

$$(4.18)$$

For the last term in (4.18), we use the Taylor expansion

$$G(\phi^{n+1}) - G(\phi^n) = G'(\phi^n)(\phi^{n+1} - \phi^n) + \frac{G''(\xi^n)}{2}(\phi^{n+1} - \phi^n)^2.$$
(4.19)

Finally, combining (4.15), (4.17), (4.18) and (4.19), and using the assumption, we obtain

$$Re(\|\mathbf{u}^{n+1}\|^{2} - \|\mathbf{u}^{n}\|^{2} + \|\tilde{\mathbf{u}}^{n+1} - \mathbf{u}^{n}\|^{2}) + 2\delta t \|\nabla \tilde{\mathbf{u}}^{n+1}\|^{2}$$

$$+ \frac{\delta t^{2}}{Re}(\|\nabla p^{n+1}\|^{2} - \|\nabla p^{n}\|^{2}) + \frac{2\delta t \mathcal{M}}{Ca} \|\nabla \mu^{n+1}\|^{2}$$

$$+ \frac{\epsilon}{Ca}(\|\nabla \phi^{n+1}\|^{2} - \|\nabla \phi^{n}\|^{2} + \|\nabla \phi^{n+1} - \nabla \phi^{n}\|^{2})$$

$$+ \frac{2s}{\epsilon Ca} \|\phi^{n+1} - \phi^{n}\|^{2} + \frac{2}{\epsilon Ca}(G(\phi^{n+1}) - G(\phi^{n}), 1)$$

$$= \frac{G''(\xi^{n})}{\epsilon Ca} \|\phi^{n+1} - \phi^{n}\|^{2} \le \frac{2s}{\epsilon Ca} \|\phi^{n+1} - \phi^{n}\|^{2}.$$

$$(4.20)$$

Taking the inner product of (4.8a) with $\delta t \mu_c^{n+1}$, we have

$$(c^{n+1} - c^n, \mu_c^{n+1}) + \delta t(\boldsymbol{u}^{n+1} \cdot \nabla c^{n+1}, \mu_c^{n+1}) + \delta t(\nabla \cdot \boldsymbol{j}^{n+1}, \mu_c^{n+1}) = 0.$$
(4.21)

Taking the inner product of (4.8b) with $\delta t \nabla \mu_c^{n+1}$, we have

$$\delta t(\nabla \mu_c^{n+1}, \mathbf{j}^{n+1}) + \delta t \int_{\Omega} D^{n+1} c^{n+1} |\nabla \mu_c^{n+1}|^2 d\mathbf{x} = 0.$$
(4.22)

Taking the inner product of (4.8c) with $c^{n+1} - c^n$, we have

$$(\mu_c^{n+1}, c^{n+1} - c^n) = (c^{n+1} - c^n, \ln c^{n+1} + 1). \tag{4.23}$$

Noting the fact that

$$c^{n} \ln c^{n} - c^{n+1} \ln c^{n+1} = -(\ln c^{n+1} + 1)(c^{n+1} - c^{n}) + \frac{1}{2\varepsilon^{n}}(c^{n+1} - c^{n})^{2}.$$

$$(4.24)$$

Combining the above four equalities, we obtain

$$(c^{n+1}\ln c^{n+1} - c^n\ln c^n, 1) + \frac{1}{2\xi^n}\|c^{n+1} - c^n\|^2 = -\delta t \int_{\Omega} D^{n+1}c^{n+1}|\nabla \mu_c^{n+1}|^2 d\mathbf{x}.$$
(4.25)

Combining (4.20) and (4.25), we have

$$\frac{Re}{2}(\|\boldsymbol{u}^{n+1}\|^{2} - \|\boldsymbol{u}^{n}\|^{2} + \|\boldsymbol{u}_{\star}^{n} - \boldsymbol{u}^{n}\|^{2} + \|\tilde{\boldsymbol{u}}^{n+1} - \boldsymbol{u}_{\star}^{n}\|^{2}) + \frac{\delta t^{2}}{2Re}(\|\nabla p^{n+1}\|^{2} - \|\nabla p^{n}\|^{2})
+ \frac{\epsilon}{2Ca}(\|\nabla \phi^{n+1}\|^{2} - \|\nabla \phi^{n}\|^{2} + \|\nabla \phi^{n+1} - \nabla \phi^{n}\|^{2}) + \frac{1}{\epsilon Ca}(G(\phi^{n+1}) - G(\phi^{n}), 1)
+ (c^{n+1}\ln c^{n+1} - c^{n}\ln c^{n}, 1) + \frac{1}{2\xi^{n}}\|c^{n+1} - c^{n}\|^{2}
= -\nu\delta t \|\nabla \tilde{\boldsymbol{u}}^{n+1}\|^{2} - \delta t \frac{\mathcal{M}}{Ca}\|\nabla \mu^{n+1}\|^{2} - \delta t \int_{\Omega} D^{n+1}c^{n+1}|\nabla \mu_{c}^{n+1}|^{2}d\boldsymbol{x}.$$
(4.26)

This completes the proof. \Box

Remark 4.1. Numerical scheme (4.4) is a coupled system for ϕ^{n+1} and $\tilde{\boldsymbol{u}}^{n+1}$. In the following numerical simulations, Block Gauss iteration method is used to solve this system and s is set to be 2 in practice.

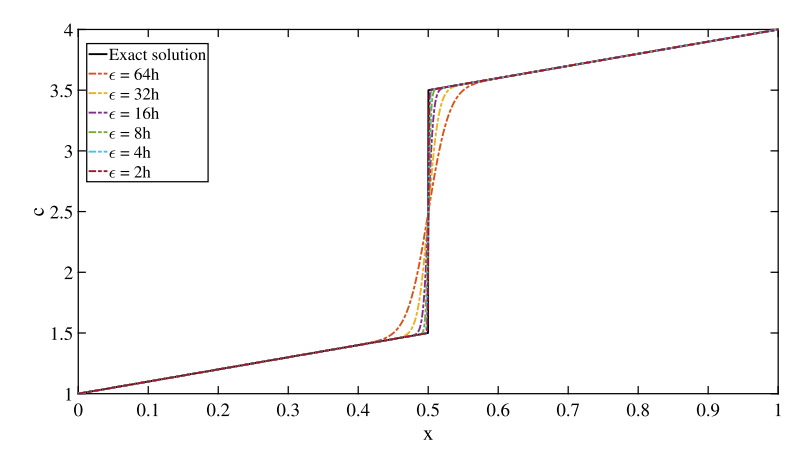


Fig. 2. Sharp interface limit test.

Table 1 The discrete L^1 error and convergence rate.

ϵ	64h	32h	16h	8h	4h	2h
L ¹ -error	3.93E-02	1.98E-02		5.13E-03	2.70E-03	1.49E-03
rate	-	0.99	0.98	0.96	0.93	0.86

5. Numerical results

In this section, numerical experiments are conducted to illustrate the validity of our model. We first check the sharp interface limit in Section 3 by choosing a relatively small value for ϵ and comparing the numerical solutions with the analytical ones when available. Then we compute the convergence rate and energy stability of the numerical scheme in Section 4. Finally, the calibrated model is applied to the problem with suspended droplets in the shear flow to study the effect of interface permeability.

Block-centered finite difference method based on stagger mesh is adopted to discretize equations (2.19) in space. Variables ϕ , c and p are located in the center of mesh, however velocity variables u and v are located on the center of edge. The main advantage of the block-centered finite difference method is that it approximates the phase function, concentration and pressure with Neumann boundary condition to second-order accuracy, as well as, it guarantees local mass conservation.

5.1. Sharp interface limit test

In this example, we consider the steady state solution in 1D to verify sharp interface limit of concentration function c. For simplicity, we first fixed the interface and only solve concentration equation (2.19e) where interface is at $x_0 = 0.5$ in domain (0, 1). The diffusion coefficient is taken as $D_1 = D_2 = 1$ and Dirichlet boundary condition $c_0 = 1$, $c_1 = 4$ is used. The exact solution model (1.1)-(1.2) is

$$c = \begin{cases} x+1, & x < x_0, \\ x+3, & x \ge x_0. \end{cases}$$
 (5.1)

In Figure 2, the exact solution is shown in black solid line and the dash lines are the solutions of Eq. (2.19e) where the phase field function is chosen as $\phi = \tanh(\frac{x-x_0}{\sqrt{2}\epsilon})$ with five different interface thickness ϵ . In the bulk region, solutions of two methods fit very well. As $\epsilon \to 0$, the proposed diffusive model solutions change much sharper near the interface and convergence to the sharp interface solution, which is consistent with our analysis in Section 5.4.1. In Table 1, we test the convergent rate of the diffuse interface model to sharp interface model under L^1 norm. A fixed spatial step as $h = \frac{1}{2048}$ is used for the different thickness of the interface ϵ . The result shows that our diffuse interface model is first order convergence to sharp interface model.

5.2. Comparison with the immersed boundary method

In this subsection, we conduct two numerical tests to compare the results using immersed boundary methods [15] and phase field method. The first experiment is 1D the steady state Eqs. (1.1)-(1.2) with Q(c) = c, K = 1/5. The locations of interfaces are chosen at $x_1 = 7/18$ and $x_2 = 11/18$, i.e. $\Omega^+ = (x_1, x_2)$ and $\Omega^- = (0, x_1) \cup (x_2, 1)$ and diffusion coefficient are $D^+ = D^- = 1$. In this case, the exact solution can be obtained as

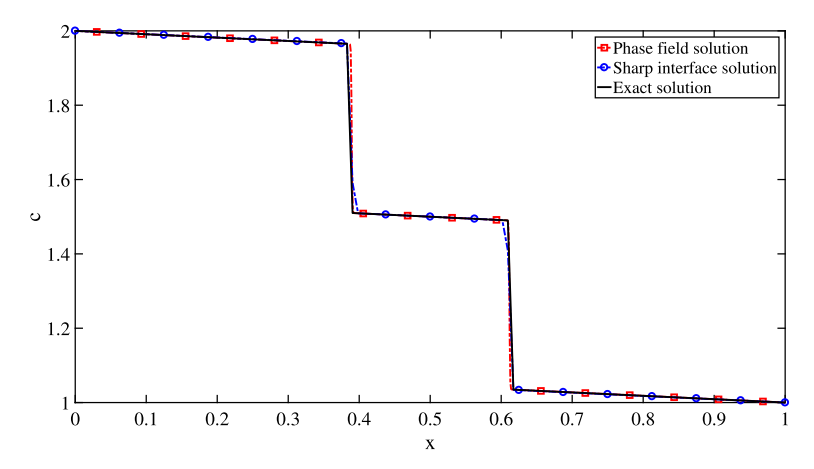


Fig. 3. Steady state solution with the linear law on the interfaces located at $x_1 = 7/18$ and $x_2 = 11/18$ with K = 0.2, D = 1, $c_0 = 2$ and $c_1 = 1$. The black solid line is the exact solution, and the red dash with square is the numerical solution by phase field method, but the blue dash with circle is the numerical solution by immersed boundary method. (For interpretation of the colors in the figure(s), the reader is referred to the web version of this article.)

$$c = \begin{cases} -\frac{1}{11}x + 2, & x < x_1, \\ -\frac{1}{11}x + \frac{17}{11}, & x_1 \le x < x_2, \\ -\frac{1}{11}(x - 1) + 1, & x \ge x_2. \end{cases}$$
 (5.2)

In Figure 3, the solid black line is the exact solution, blue line with circle is the immersed boundary solution and the red line with square is the phase field solution with interface width $\epsilon=0.01$. We can see that the numerical both solutions agree with the exact solution.

In the second example, the interface is fixed as a circle with radius r = 11/18 and center at $\mathbf{x}_0 = (0.5, 0.5)$. The initial condition of the concentration (see Fig. 4 (a)) and parameters are set to be same as those in [15], $c(t_0, \mathbf{x}) = G(t_0, \mathbf{x} - \mathbf{x}_0)$, where

$$G(t, \mathbf{x} - \mathbf{x}_0) = \frac{1}{4\pi Dt} \exp\left(-\frac{\mathbf{x} - \mathbf{x}_0}{4Dt}\right). \tag{5.3}$$

with

$$t_0 = 10^{-4}, \quad D = 1, \quad K = 10.$$
 (5.4)

The computational domain is discretized by a uniform grid with size 1/128 and interface thickness $\epsilon = 0.01$.

Fig. 4 (b) shows the contour lines of concentrations by using immersed boundary (dash lines) [15] and phase field methods (solid lines) at time $t = t_0 + 10^{-2}$. It indicates that our diffusive interface model solutions agrees with the immerse interface results.

5.3. Comparison with experimental results

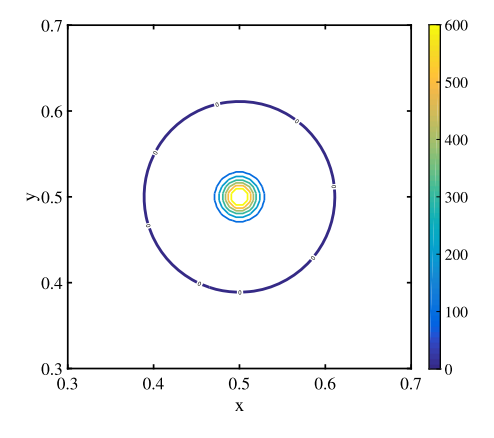
In this section, we calibrate our phase field model with an experimental study on drug delivery in [16]. To model the penetration of nanoparticles into the tumor, we can use our restricted diffusion framework. For simplicity, we only consider the effect of cell membrane on particles penetration and the effect of fluid flow and deformation of cells are neglected.

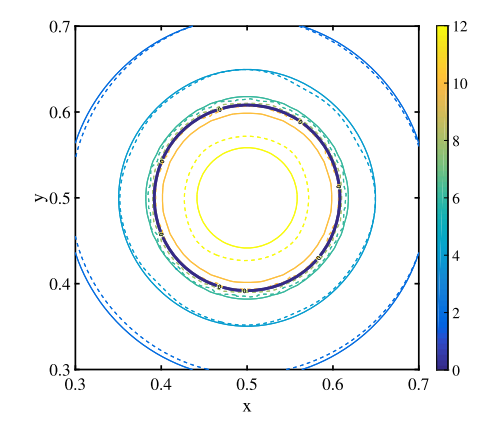
As shown in Fig. 5, fixed cells with an interface thickness $\delta = 0.005$ and the radius r = 0.04 are arranged in the domain as $\Omega = Lx \times Ly = [0, 1] \times [0, 0.2]$, using label function ϕ as follows,

$$\phi(\mathbf{x},0) = \sum_{i=0}^{4} \sum_{j=0}^{2} \left(\tanh \frac{r - \sqrt{(x - (\frac{1}{20}Lx + \frac{i}{5}Lx))^{2} + (y - \frac{j}{2}Ly)^{2}}}{\sqrt{2}\epsilon} + 1.0 \right)$$

$$+ \sum_{i=0}^{4} \sum_{j=0}^{1} \left(\tanh \frac{r - \sqrt{(x - (\frac{1}{20}Lx + \frac{2i+1}{10}Lx))^{2} + (y - (\frac{1}{4}Ly + \frac{j}{2}Ly))^{2}}}{\sqrt{2}\epsilon} + 1.0 \right) - 1.0.$$
 (5.5a)

The nanoparticles concentration is initially set to be c(x, 0) = 0 with boundary condition





- (a) Initial condition of concentration.
- (b) Snapshot of level curves of concentration at $t = t_0 + 10^{-2}$.

Fig. 4. Comparison between phase field method and immersed boundary method for mass transfer. The fixed interface is expressed with bold cure marked by 0. (a): The initial condition of concentration that concentrates in the centre. (b): Snapshot of level curves of concentration $t = t_0 + 10^{-2}$ by using different methods. The dashed lines are level curves obtained by immersed boundary method [15] and the solid lines are the level curves obtained by proposed diffusive interface method.

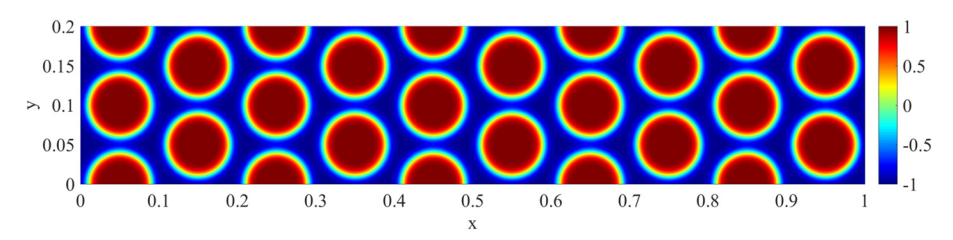


Fig. 5. Initial setting of the cells.

$$c(x=0) = 1, \quad c(x=1) = 0, \quad \nabla c \cdot \mathbf{n}|_{v=0} = \nabla c \cdot \mathbf{n}|_{v=0,2} = 0.$$
 (5.6)

The parameters are

$$D^{+} = 1, \quad D^{-} = 18, \quad K = 1,$$
 (5.7)

to model the effects of cell permeability on distribution and penetration of drug in biological tissues in [16,40].

In Figs. 6 and 7, we present the concentrations at the steady states with q = 1 - c and $q = (1 - c)^2$. The latter case fits better with the experimental data in [16].

5.4. Convergence and unconditional energy stability

In this section, we conduct convergence and unconditional energy stable tests to illustrate the effectiveness of our proposed numerical scheme. Here we use the a uniform mesh with the mesh size $N_x = N_y = N$.

5.4.1. Convergence rate

We use a uniform Cartesian grid to discretize a square domain $\Omega=(0,1)^2\subset\mathbb{R}^2$. The initial condition is chosen as follows.

$$\phi(\mathbf{x}, 0) = 0.2 + 0.5\cos(2\pi x)\cos(2\pi y),\tag{5.8a}$$

$$c(\mathbf{x}, 0) = 0.6 + 0.2\cos(2\pi x)\cos(2\pi y),\tag{5.8b}$$

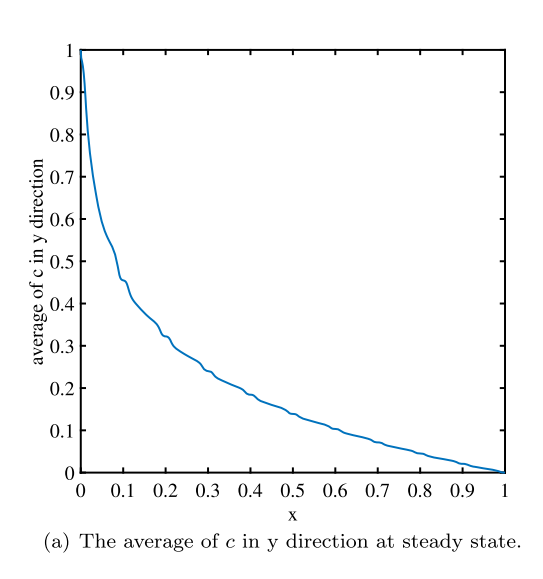
$$u(\mathbf{x},0) = -0.25\sin^2(\pi x)\cos(2\pi y),\tag{5.8c}$$

$$v(\mathbf{x},0) = 0.25\sin^2(\pi y)\cos(2\pi x). \tag{5.8d}$$

Periodic boundary conditions are used for all variables. The parameters in model (2.19) are set as

$$\epsilon = 0.08, \quad Re = 1, \quad Ca = 1, \quad Pe = 1, \quad D^+ = D^- = 1, \quad K = A^{-1}, \quad Q(c) = c.$$
 (5.9)

The Cauchy error [35] is computed to test the convergence rate, where error between two different spacial mesh sizes h and h/2 is calculated by $\|e_{\zeta}\| = \|\zeta_h - \zeta_{h/2}\|$, for the solution ζ . The mesh sizes are set to be h = 1



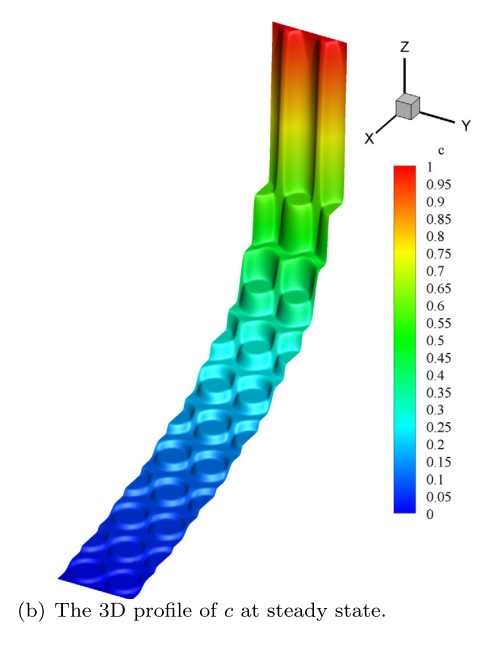
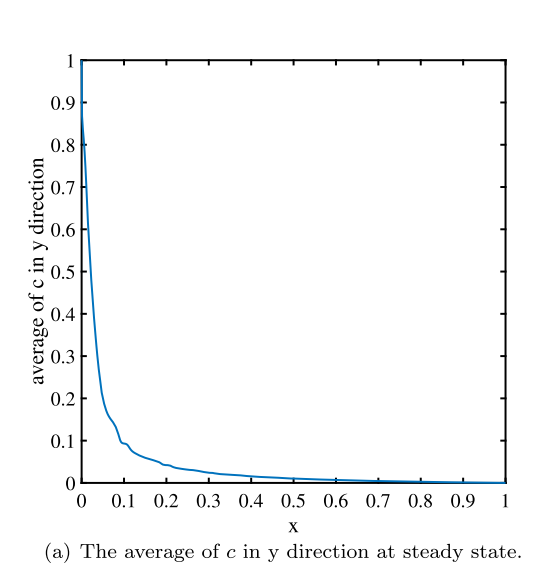


Fig. 6. Profile of c at steady state with q = 1 - c.



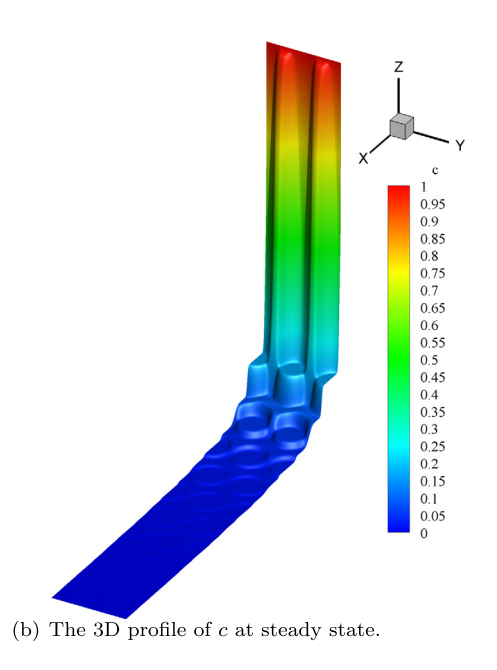


Fig. 7. Profile of *c* at steady state with $q = (1 - c)^2$.

1/16, 1/32, 1/64, 1/128, 1/256 and time step is fixed at $\delta t = 10^{-4}$. The L^2 and L^{∞} numerical errors and convergence rate at time T = 0.1 are displayed in Table 2 and Table 3, respectively. The second order spatial accuracy is apparently for all the variables.

5.4.2. Unconditionally energy stable test

In this subsection, we carry out a numerical experiment to survey the unconditionally energy stability about our numerical scheme with the same initial condition and boundary conditions. The result is listed in Figure 8. Time steps are chosen from $\delta t = 0.1$ to $\delta t = 0.1 \times \frac{1}{2^8}$ with fixed spacial mesh size h = 1/128.

The total energy over time with different time steps are shown in Fig. 8. It illustrates that energy is monotonic decrease

as time step is reduced, which confirms the unconditional energy stability of the proposed scheme.

Table 2 The discrete L^2 error and convergence rate at t = 0.1 with initial data (5.8) and the given parameters.

Grid sizes	Error (φ)	Rate	Error (c)	Rate	Error (u)	Rate	Error (v)	Rate	Error (p)	Rate
16 × 16	4.01e-02	-	1.01e-02	-	1.15e-04	-	1.15e-04	-	1.57e-03	-
32×32	8.90e-03	2.17	4.91e-03	1.90	3.23e-05	1.83	3.23e-05	1.83	1.24e-04	3.66
64×64	2.22e-03	2.01	6.80e-04	1.99	8.06e-06	2.00	8.06e-06	2.00	3.00e-05	2.05
128×128	5.54e-04	2.00	1.70e-04	2.00	2.01e-06	2.00	2.01e-06	2.00	7.46e-06	2.01
256×256	1.38e-04	2.00	4.26e-05	2.00	5.04e-07	2.00	5.04e-07	2.00	1.86e-06	2.00

Table 3 The discrete L^{∞} error and convergence rate at t = 0.1 with initial data (5.8) and the given parameters.

Grid sizes	Error (ϕ)	Rate	Error (c)	Rate	Error (u)	Rate	Error (v)	Rate	Error (p)	Rate
16 × 16	7.64e-02	-	1.89e-02	-	1.83e-04	-	1.83e-04	-	3.99e-03	_
32×32	1.69e-02	2.17	4.91e-03	1.95	5.00e-05	1.88	5.00e-05	1.88	2.53e-04	3.98
64×64	4.18e-03	2.02	1.23e-03	1.99	1.25e-05	2.00	1.25e-05	2.00	5.89e-05	2.10
128×128	1.03e-03	2.02	3.07e-04	2.01	3.12e-06	2.00	3.12e-06	2.00	1.50e-05	1.98
256×256	2.55e-04	2.01	7.61e-05	2.01	7.80e-07	2.00	7.80e-07	2.00	3.71e-06	2.01

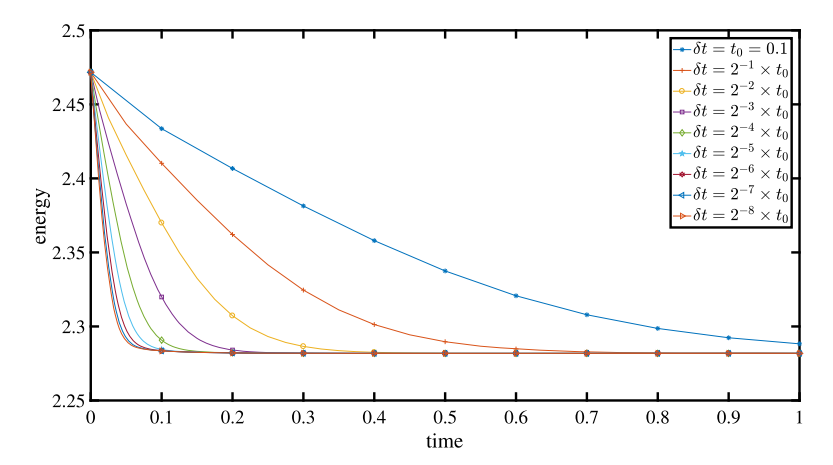


Fig. 8. Unconditional energy stability with different time steps represented by different markers and colors.

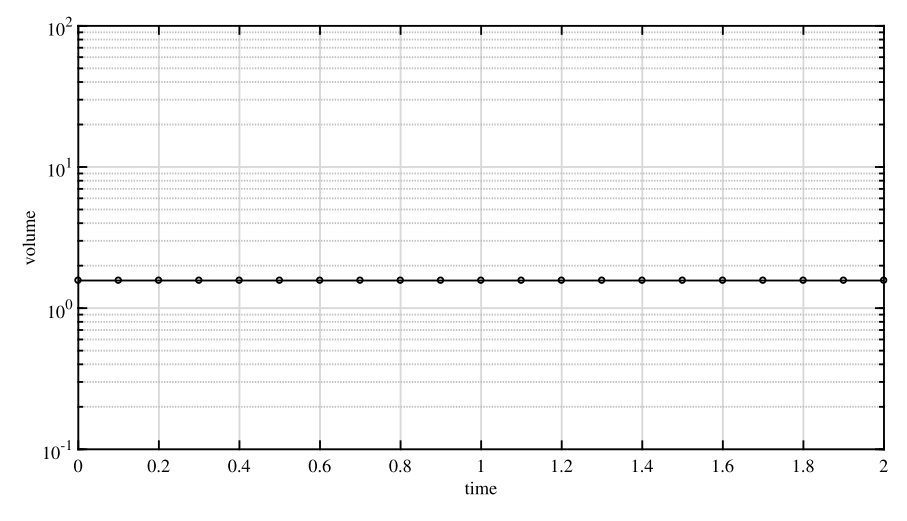


Fig. 9. Conservation of volume of the numerical scheme with time step $\delta t = 0.1 \times 2^{-8}$.

We utilize the result computed with time step $\delta t = 0.1 \times \frac{1}{2^8}$ to verify conservation of volume in Fig. 9. This result demonstrates the volume of ϕ is conserved over time.

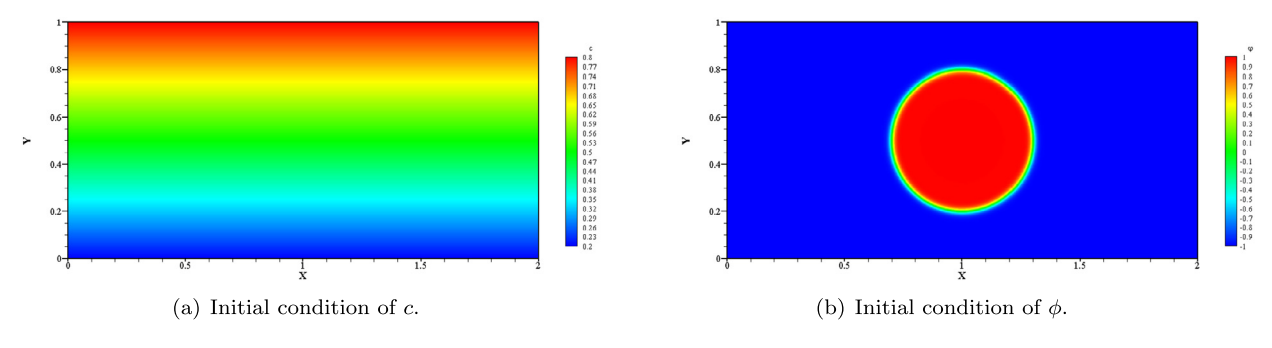


Fig. 10. Initial condition for Example 5.10. We set the concentration as a linear function in the y direction.

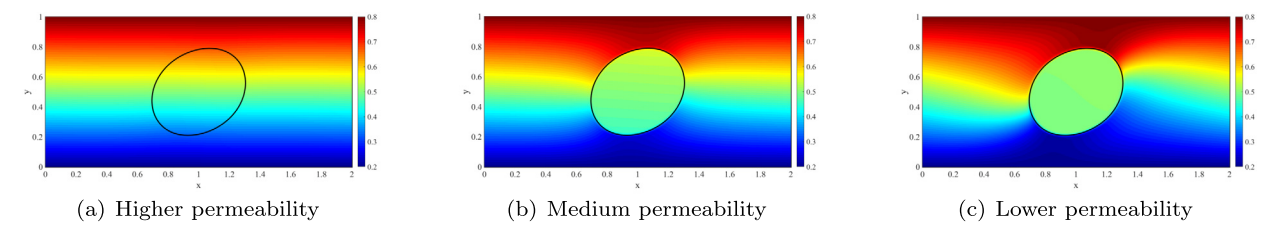


Fig. 11. Snapshots of c at steady state with different permeability: $K = \frac{1}{2\sigma\delta}, \frac{1}{2\sigma}$ and $\frac{\delta}{2\sigma}$.

5.5. Effect of interface permeability

We first consider a single drop with high $(K = \frac{1}{2\sigma\delta})$, medium $(K = \frac{1}{2\sigma})$ and low $(K = \frac{\delta}{2\sigma})$ permeability with $\delta = 0.01$, is suspended in a shear flow. The initial profiles of concentration and interface are given as follows (see Fig. 10),

$$\phi(\mathbf{x},0) = \tanh \frac{0.25 - \sqrt{(x - 0.5)^2 + (y - 0.5)^2}}{\sqrt{2}\epsilon},\tag{5.10a}$$

$$c(\mathbf{x}, 0) = 0.6y + 0.2,$$
 (5.10b)

with boundary condition

$$\nabla \phi \cdot \mathbf{n}|_{y=0} = \nabla \phi \cdot \mathbf{n}|_{y=1} = 0, \quad \phi(0, y, t) = \phi(1, y, t),$$

$$\nabla \mu \cdot \mathbf{n}|_{y=0} = \nabla \mu \cdot \mathbf{n}|_{y=1} = 0, \quad \mu(0, y, t) = \mu(1, y, t),$$

$$\nabla c \cdot \mathbf{n}|_{y=0} = \nabla c \cdot \mathbf{n}|_{y=1} = 0, \quad c(0, y, t) = c(1, y, t),$$

$$\mathbf{u}|_{y=0} = (-1, 0)^{T}, \quad \mathbf{u}|_{y=1} = (1, 0)^{T},$$

and periodic boundary conditions are used on the left and right boundaries. The parameters are given as

$$Re = 1$$
, $Ca = 0.1$, $Pe = 1$, $D^{+} = 1$, $D^{-} = 1$, $\epsilon = 0.01$, $\mathcal{M} = 10^{-4}$. (5.11)

The 2D and 3D profiles of concentration at steady states are shown in Figs. 11,12. For a interface with relative large permeability, the distribution of concentration is almost the linear. This could also be observed by the direction of flux in Fig. 13 (a) and magnitude of flux in Fig. 15(a). When the permeability decreases, the flux across the interface decreases (see Fig. 15(b-c) and Fig. 13(b-c)). Fig. 14 illustrates this restriction does not effect the water flow pattern at the steady state since water is not permeable for the interface in this work. At the steady state, due to limited flux through the interface, the concentration inside the inner region Ω^+ is nearly uniform (see Figs. 11,12 (c)) due to diffusion, while the profile of concentration in the out region Ω^- is similar to that of diffusion in a perforated domain.

In the next, we consider the case with two droplets suspended in the shear flow with a rectangular area $\Omega = [0, 2] \times [0, 1]$. The initial condition for ϕ is given by

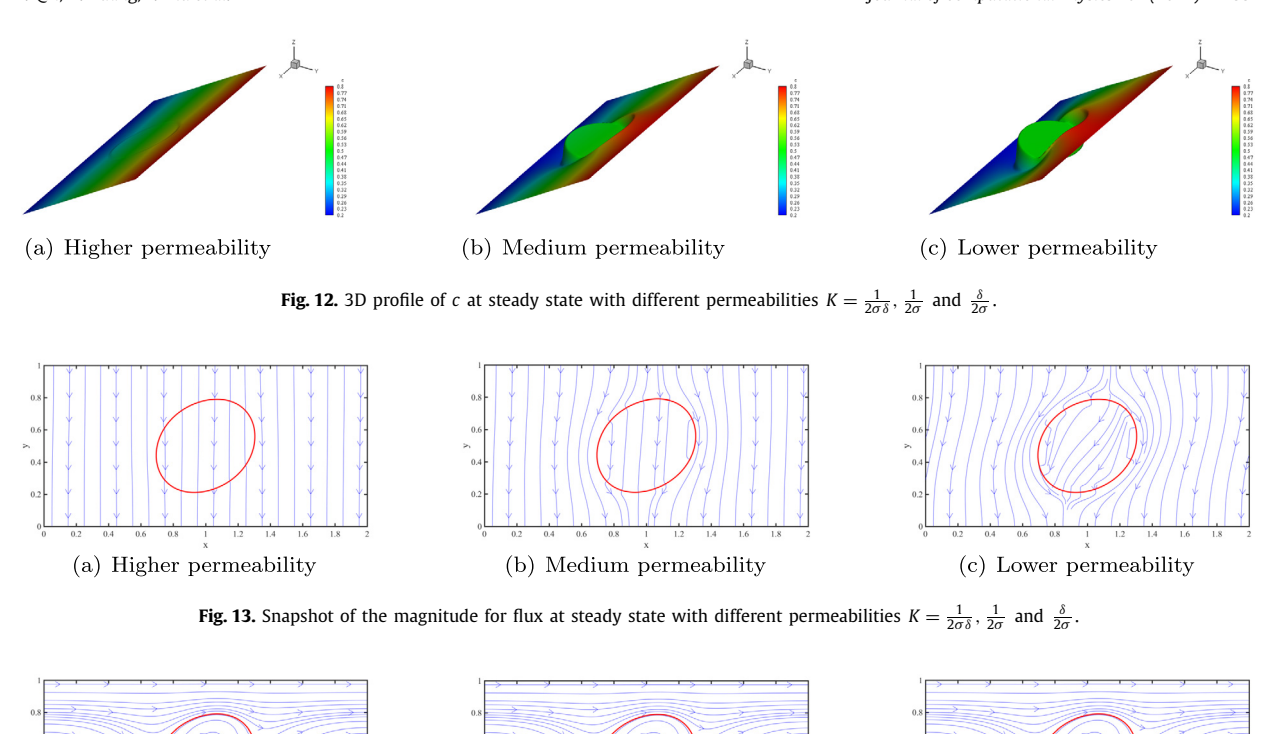
$$\phi(\mathbf{x},0) = \tanh\left(\frac{0.2 - \sqrt{(x - 0.5)^2 + (y - 0.7)^2}}{\sqrt{2}\epsilon}\right) + \tanh\left(\frac{0.2 - \sqrt{(x - 1.5)^2 + (y - 0.3)^2}}{\sqrt{2}\epsilon}\right) + 1.0,\tag{5.12}$$

and the parameters are

$$Re = 100$$
, $Ca = 1$, $Pe = 1$, $D^{+} = D^{-} = 1$, $\epsilon = 0.02$, $\mathcal{M} = 0.02$.

(a) Higher permeability

(c) Lower permeability



meability (b) Medium permeability (c) Lowe Fig. 14. Snapshot of the streamline at steady state with different permeabilities $K = \frac{1}{2\sigma\delta}, \frac{1}{2\sigma}$ and $\frac{\delta}{2\sigma}$.

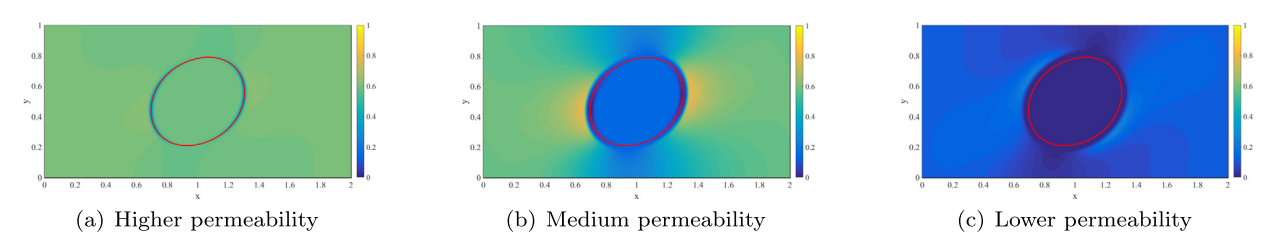


Fig. 15. Snapshot of the magnitude for flux at steady state with different permeabilities $K = \frac{1}{2\sigma\delta}, \frac{1}{2\sigma}$ and $\frac{\delta}{2\sigma}$.

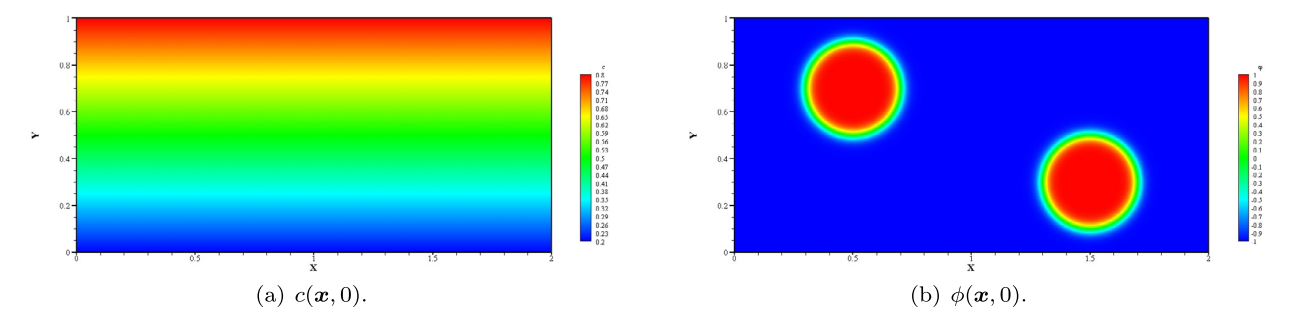


Fig. 16. Profile of initial condition.

The permeability is chosen as $K = \frac{1}{2\sigma}$. The initial conditions of c and u and all the other parameters are chosen the same as in the previous example (5.10). The initial profiles of concentration and droplets are shown in Fig. 16

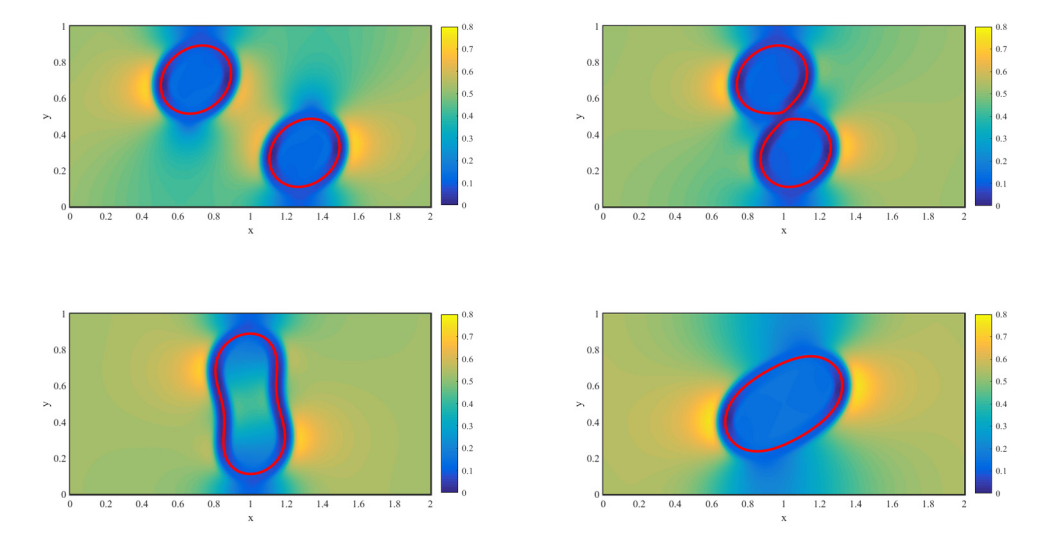


Fig. 17. Evolution of the magnitude for flux at different time t = 0.5, t = 1.1, t = 1.2 and t = 5.0. The red circles show the location of membrane.

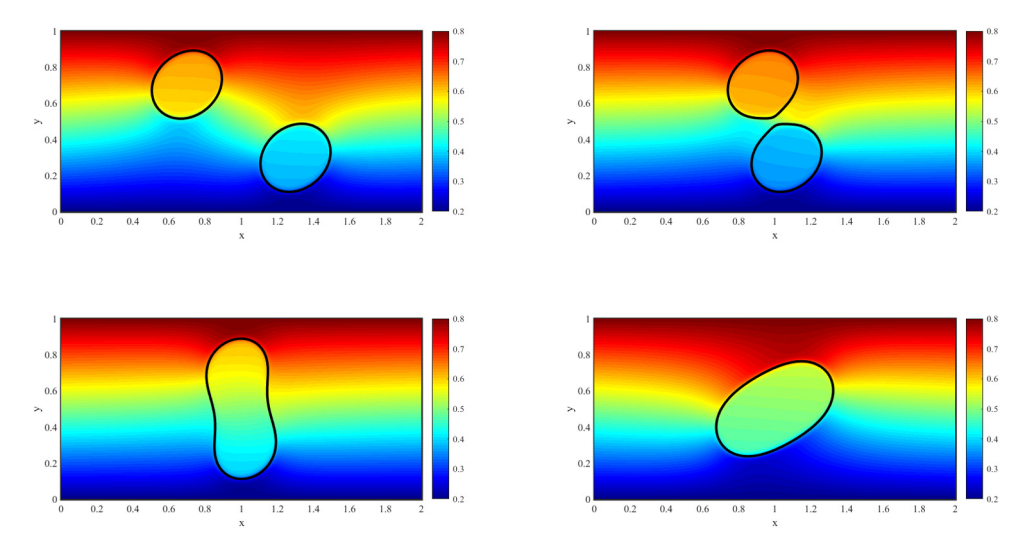


Fig. 18. Evolution of the concentration at different time t = 0.5, t = 1.1, t = 1.2 and t = 5.0. The black circles show the location of membrane.

In Fig. 17, the magnitude of flux overtime are plotted. Due to the shear flow, the droplets move closer and merge into one droplet around time t = 1.2. Before t = 1.2, the restrict diffusion are observed on two interface. After the merge time, the droplet achieves new equilibrium of concentration, where the inner region flux is close to zero.

Fig. 18 reveals the evolution of concentration. We can see there is a concentration difference between inside and outside of membrane because of the restrict diffusion.

6. Conclusions

In this paper, we propose a phase field model for mass transfer through a semi-permeable membrane with the restricted diffusion, coupled with fluid flows. The derivation is based on energy variation method and thermally consistent. The sharp interface limit is obtained by using asymptotic analysis and supported by numerical simulations. Our results show that as the interface thickness approaches to zero, the diffusive interface model converges to the sharp interface one. We established a linear and unconditional energy stable numerical scheme to solve the model equations, which form a coupled nonlinear system. The centered-block finite difference method with a staggered grid is used for spacial discretization. Numerical computations are carried out to study to the effect of interface permeability. The results show that our diffusive interface model could be applied to solve restricted diffusion problems efficiently and handle interface topological changes easily.

Both Immersed Boundary Method and Phase Field Method are carried out on Cartesian grids and simplicity to implement for fluid-structure interaction problems. Immersed Boundary Method has the principal advantage that it can use a large number of interfacial marker points to accurately handle the interface geometry. However, it is the difficulty of topological

change unless the additional work for geometric problems is considered [14]. The first advantages of Phase Field method is that it follows energy dissipation law such that we could design energy stability schemes for long time simulations. The other advantages is that Phase Field method could easily handle the topological changes, like merging and breaking. However, it is not easy to handle open curve problems [7].

In this paper, we mainly focus on the passive flux of neutral particles, which is determined by difference on both sides of interface. The restricted diffusion through biological membrane may also evolve absorption or electrical properties, such as capacitance and resistance, and active pumps to maintain the concentration difference [44,16]. In Section 5.3, we only considered the simplest case. In the future, coupling with the Poisson-Nernst-Planck [38], the penetration of charged nanoparticles through deformable tissue cells under fluid will be studied to compare with the experiment data.

CRediT authorship contribution statement

Zheyu Qin: Model derivation; Simulations; Manuscript draft. **Huaxiong Huang:** Project design; Manuscript revision. **Yi Zhu:** Model derivation. **Chun Liu:** Model derivation. **Shixin Xu:** Model derivation; Project design and coordination; Manuscript draft and revision.

Declaration of competing interest

The authors declare that they have no known competing financial interests or personal relationships that could have appeared to influence the work reported in this paper.

Acknowledgement

This work was partially supported by the National Natural Science Foundation of China no. 12071190 and Natural Sciences and Engineering Research Council of Canada (NSERC). We thank Prof. Robert Eisenberg for suggestions and helpful discussions. We also would like to thank American Institute of Mathematics where this project initiated.

References

- [1] D. Adalsteinsson, J.A. Sethian, A fast level set method for propagating interfaces, J. Comput. Phys. 118 (2) (1995) 269-277.
- [2] L.A. Caffarelli, N.E. Muler, An L^{∞} bound for solutions of the Cahn-Hilliard equation, Arch. Ration. Mech. Anal. 133 (1995) 129–144.
- [3] J.W. Cahn, Free energy of a nonuniform system. II. thermodynamic basis, J. Chem. Phys. 30 (5) (1959) 1121-1124.
- [4] J.W. Cahn, J.E. Hilliard, Free energy of a nonuniform system. I. Interfacial free energy, J. Chem. Phys. 28 (2) (1958) 258-267.
- [5] J.W. Cahn, J.E. Hilliard, Free energy of a nonuniform system. III. Nucleation in a two component incompressible fluid, J. Chem. Phys. 31 (3) (1959) 688–699.
- [6] A.J. Chorin, Numerical solution of the Navier-Stokes equations, Math. Comput. 22 (104) (1968) 745-762.
- [7] F.S. Cohen, R. Eisenberg, R.J. Ryham, A dynamic model of open vesicles in fluids, Commun. Math. Sci. 10 (4) (2012) 1273-1285.
- [8] M.R. Davidson, M. Rudman, Volume-of-fluid calculation of heat or mass transfer across deforming interfaces in two-fluid flow, Numer. Heat Transf., Part B, Fundam. 41 (3–4) (2002) 291–308.
- [9] B. Eisenberg, Y. Hyon, C. Liu, Energy variational analysis of ions in water and channels: Field theory for primitive models of complex ionic fluids, J. Chem. Phys. 133 (10) (2010) 104104.
- [10] X. Feng, T. Tang, J. Yang, Stabilized Crank-Nicolson/Adams-Bashforth schemes for phase field models, East Asian J. Appl. Math. 3 (1) (2013) 59-80.
- [11] G.L. Flynn, S.H. Yalkowsky, T.J. Roseman, Mass transport phenomena and models: theoretical concepts, J. Pharm. Sci. 63 (4) (1974) 479-510.
- [12] X. Gong, Z. Gong, H. Huang, An immersed boundary method for mass transfer across permeable moving interfaces, J. Comput. Phys. 278 (2014) 148–168.
- [13] J.L. Guermond, P. Minev, J. Shen, An overview of projection methods for incompressible flows, Comput. Methods Appl. Mech. Eng. 195 (44–47) (2006) 6011–6045
- [14] H. Hua, J. Shin, J. Kim, Level set, phase-field, and immersed boundary methods for two-phase fluid flows, J. Fluids Eng. 136 (2) (2014).
- [15] H. Huang, K. Sugiyama, S. Takagi, An immersed boundary method for restricted diffusion with permeable interfaces, J. Comput. Phys. 228 (15) (2009) 5317–5322.
- [16] K. Huang, R. Boerhan, C. Liu, G. Jiang, Nanoparticles penetrate into the multicellular spheroid-on-chip: effect of surface charge, protein corona, and exterior flow, Mol. Pharm. 14 (12) (2017) 4618–4627.
- [17] H. Jiang, S.X. Sun, Cellular pressure and volume regulation and implications for cell mechanics, Biophys. J. 105 (3) (2013) 609-619.
- [18] J. Johansson, C.P.T. Svensson, T. Mårtensson, L. Samuelson, W. Seifert, Mass transport model for semiconductor nanowire growth, J. Phys. Chem. B 109 (28) (2005) 13567–13571.
- [19] A.T. Layton, Modeling water transport across elastic boundaries using an explicit jump method, SIAM J. Sci. Comput. 28 (6) (2006) 2189-2207.
- [20] R.J. LeVeque, Z. Li, Immersed interface methods for stokes flow with elastic boundaries or surface tension, SIAM J. Sci. Comput. 18 (3) (1997) 709–735.
- [21] X. Li, W. Wang, P. Zhang, J. Li, G. Chen, Interactions between gas-liquid mass transfer and bubble behaviours, R. Soc. Open Sci. 6 (5) (2019) 190136.
- [22] A.G. Pakhomov, A.M. Bowman, B.L. Ibey, F.M. Andre, O.N. Pakhomova, K.H. Schoenbach, Lipid nanopores can form a stable, ion channel-like conduction pathway in cell membrane, Biochem. Biophys. Res. Commun. 385 (2) (2009) 181–186.
- [23] C.S. Peskin, The immersed boundary method, Acta Numer. 11 (2002) 479-517.
- [24] R.J. Ryham, An energetic variational approach to mathematical modeling of charged fluids: charge phases, simulation and well posedness, 2006.
- [25] J. Shen, X. Yang, Energy stable schemes for Cahn-Hilliard phase-field model of two-phase incompressible flows, Chin. Ann. Math., Ser. B 31 (2010) 743–758.
- [26] J. Shen, X. Yang, Numerical approximations of Allen-Cahn and Cahn-Hilliard equations, Discrete Contin. Dyn. Syst. 28 (4) (2010) 1669–1691.
- [27] J. Shen, X. Yang, Decoupled, energy stable schemes for phase-field models of two-phase incompressible flows, SIAM J. Numer. Anal. 53 (1) (2015) 279–296.

- [28] L. Shen, H. Huang, P. Lin, Z. Song, S. Xu, An energy stable c0 finite element scheme for a quasi-incompressible phase-field model of moving contact line with variable density, J. Comput. Phys. 405 (2020) 109179.
- 1291 I.S. Sohn, Y. Tseng, S. Li, A. Voigt, I.S. Lowengrub, Dynamics of multicomponent vesicles in a viscous fluid, I. Comput, Phys. 229 (1) (2010) 119-144.
- [30] Z. Song, X. Cao, H. Huang, Electroneutral models for a multidimensional dynamic Poisson-Nernst-Planck system, Phys. Rev. E 98 (3) (2018) 032404.
- [31] S.O. Unverdi, G. Tryggvason, A front-tracking method for viscous, incompressible, multi-fluid flows, J. Comput. Phys. 100 (1) (1992) 25-37.
- [32] J.D. van der Waals, The thermodynamic theory of capillarity under the hypothesis of a continuous variation of density, J. Stat. Phys. 20 (1893) 197-244.
- [33] X. Wang, X. Gong, K. Sugiyama, S. Takagi, H. Huang, An immersed boundary method for mass transfer through porous biomembranes under large deformations, J. Comput. Phys. 413 (2020) 109444.
- [34] S.W.J. Welch, J. Wilson, A volume of fluid based method for fluid flows with phase change, J. Comput. Phys. 160 (2) (2000) 662-682.
- [35] S. Wise, J. Kim, J. Lowengrub, Solving the regularized, strongly anisotropic Cahn-Hilliard equation by an adaptive nonlinear multigrid method, J. Comput. Phys. 226 (1) (2007) 414-446.
- [36] C. Xu, T. Tang, Stability analysis of large time-stepping methods for epitaxial growth models, SIAM J. Numer. Anal. 44 (2006) 1759-1779.
- [37] S. Xu, B. Eisenberg, Z. Song, H. Huang, Osmosis through a semi-permeable membrane: a consistent approach to interactions, arXiv preprint, arXiv: 1806.00646, 2018.
- [38] Shixin Xu, Ping Sheng, Chun Liu, An energetic variational approach for ion transport, arXiv preprint, arXiv:1408.4114, 2014.
- [39] X. Xu, Y. Di, H. Yu, Sharp-interface limits of a phase-field model with a generalized Navier slip boundary condition for moving contact lines, J. Fluid Mech. 849 (2018) 805–833.
- [40] K.S. Yadav, D.C. Dalal, Effects of cell permeability on distribution and penetration of drug into biological tissues: A multiscale approach, Appl. Math. Model. 108 (2022) 355–375.
- [41] P. Yue, J.J. Feng, C. Liu, J. Shen, A diffuse-interface method for simulating two-phase flows of complex fluids, J. Fluid Mech. 515 (2004) 293.
- [42] H. Zhang, Z. Shen, B. Hogan, A.I. Barakat, C. Misbah, ATP release by red blood cells under flow: model and simulations, Biophys. J. 115 (11) (2018) 2218–2229.
- [43] J. Zhu, L. Chen, J. Shen, V. Tikare, Coarsening kinetics from a variable-mobility Cahn-Hilliard equation: Application of a semi-implicit Fourier spectral method, Phys. Rev. E 60 (4) (1999) 3564–3572.
- [44] Y. Zhu, S. Xu, R.S. Eisenberg, H. Huang, A bidomain model for lens microcirculation, Biophys. J. 116 (6) (2019) 1171-1184.